Design, Optimization, and Characterization of Lactoferrin-loaded Chitosan/TPP and Chitosan/Sulfobutylether-β-cyclodextrin Nanoparticles as a Pharmacological Alternative for Keratoconus Treatment

Rubén Varela-Fernández[1,2], Xurxo García-Otero[1,3], Victoria Díaz-Tomé[1], Uxía Regueiro[2], Maite López-López[2], Miguel González-Barcia[4], María Isabel Lema[5,*], and Francisco Javier Otero-Espinar[1,6,*].

1. Department of Pharmacology, Pharmacy and Pharmaceutical Technology. University of Santiago de Compostela (USC). Campus vida. Santiago de Compostela. Zip Code: 15782. Spain. francisco.otero@usc.es.

2. Clinical Neurosciences Group. University Clinical Hospital, Health Research Institute of Santiago de Compostela (IDIS). Travesía da Choupana s/n Santiago de Compostela. Zip Code: 15706. Spain. rubenvf1@gmail.com.

3. Molecular Imaging Group. University Clinical Hospital, Health Research Institute of Santiago de Compostela (IDIS). Travesía da Choupana s/n Santiago de Compostela. Zip Code: 15706. Spain. xurxo.garcia.otero@gmail.com

4. Clinical Pharmacology Group. University Clinical Hospital, Health Research Institute of Santiago de Compostela (IDIS). Travesía da Choupana s/n Santiago de Compostela. Zip Code: 15706. Spain. miguel.gonzalez.barcia@sergas.es.

5. Department of Surgery and Medical-Surgical Specialties. Ophthalmology Area. University of Santiago de Compostela (USC).Campus Vida. Santiago de Compostela. Zip Code: 15706. Spain. mariaisabel.lema@usc.es.

6. Paraquasil Group. University Clinical Hospital, Health Research Institute of Santiago de Compostela (IDIS). Travesía da Choupana s/n Santiago de Compostela. Zip Code: 15706. Spain. francisco.otero@usc.es.

KEYWORDS Nanoparticles, Chitosan, Sulfobutylether- -cyclodextrin, Tripolyphosphate, Lactoferrin, Topical ophthalmic administration, Protein nanocarriers, Keratoconus

ABSTRACT: This research study describes the design, optimization, and characterization of two different types of chitosan-based nanoparticles as novel drug delivery systems of a protein drug, lactoferrin. A preclinical consistent base was obtained for both nanosystems, being considered as the first pharmacological treatment for keratoconus as an alternative to current invasive clinical methods. Both types of nanoparticles were obtained via the ionotropic gelation technique. The size and morphology of the nanoparticles were studied as a function of the preparation conditions. A mean size of 180.73 ± 40.67 nm, a size distribution (PDI) of 0.170 ± 0.067 and positive potential values, ranging from 17.13 to 19.89 mV were achieved. Lactoferrin was successfully incorporated into both types of nanocarriers. *In vitro* release profiles showed a lactoferrin enhanced, prolonged and controlled delivery from the polymeric matrix. These formulations also demonstrated no stability or cytotoxicity problems, as well as appropriate mucoadhesive properties, with a high permanence time in the ocular surface. Thus, both types of nanoparticles may be considered as nanocarriers for the controlled release of lactoferrin as novel topical ophthalmic drug delivery systems.

INTRODUCTION

Conventional administration routes have been the preferential methods for drug release in the management of ocular pathologies (1). Nevertheless, micro and nanoparticles developed in the past decades are becoming the most promising ocular drug delivery systems (DDS), showing a great therapeutic potential because of their ability to shelter drugs from degradation, enhance ocular penetration and modulate or control drug pharmacokinetics. As a result, an

efficacy improvement, a drug toxicity reduction and an upsurge in the residence time in the target tissue were observed (2).

The ability of prolonging the drug release to the target tissue makes these carriers more attractive since they can reduce the rate of administration, also improving patient compliance to treatment. A more recent strategy based on the incorporation of cyclodextrins (CDs) in nanometric carriers has risen in the past decades. Its aim is focused in the design of versatile DDS that are able to encapsulate drugs with unfavorable physicochemical properties (3).

Keratoconus is a progressive bilateral degenerative corneal ectasia that affects young adults, causing great visual disability, with great impact on life quality and social health, worsening over time (4). The keratoconus prevalence established from 1/2000 in the worldwide population, has evolved to higher rates in several countries with the development of topographic and corneal tomographic techniques that allow an earlier diagnosis (5).

There is no available medical or pharmacological treatment to prevent the development or decrease the progression of this disease. Besides, the optical treatment for visual rehabilitation (glasses or contact lenses) in initial and moderate stages does not stop the ectasia progression, making it necessary to recur to implanting intracorneal ring segments (ICRS) or corneal transplant in advanced stages, with limited visual recovery (6). Currently, the only conservative treatment that has proven effectiveness in slowing or delaying the keratoconus progression was corneal cross linking (CXL). However, CXL is only being performed in progressive stages with visual impairment, and it is not effective in all cases, possibly due to the exclusive use of topographical criteria (7).

Despite the high prevalence of the disease and the visual disability that it causes from an early age, both the etiology and progression determinant factors remain unclear. Besides that, its etiology appears to be multifactorial or represents the final common path of different pathological processes (8).

The corneal tissue degeneration in progressive keratoconus comprises the expression of inflammatory and immune intermediaries, including cytokines, proteases and other molecules. Furthermore, a decrease in lactoferrin lacrimal levels in patients with keratoconus was observed (9). Resulting outcomes propose the immunological processes as the main core in the ecstatic disorder pathogenesis.

Lactoferrin (Lf) is an 80 kDa iron-binding glycoprotein that has shown different biological effects (10). Corneally, Lf was observed to promote *in vivo* and *in vitro* corneal epithelial wound healing (11). The innate and adaptive reactions of the immunological system may be also modulated by this protein by promoting changes in the humoral and cellular components, as well as inducing extracellular and intracellular signaling pathways involving Toll-Like receptors (TLRs), which regulate the gene expression of cytokines and other inflammatory mediators (12). Recently, our group confirmed the TLR2-4 receptors overexpression in the myeloid line cells (monocytes and neutrophils) of keratoconus patients, as well as a decrease in Lf lacrimal levels (13,14).

Two important criteria (corneal contact time and drug penetration) should be taken into account in a topical ophthalmic formulation that improve ocular bioavailability. Novel DDS are required for ocular drug delivery due to the numerous disadvantages of the conventional ocular dosage forms.

Previous studies (15) have confirmed that small proteins (M_w < 66 kD) showed a slow diffusion rate through the excised corneal tissue (100-fold slower than glucose). Consequently, a low Lf diffusion rate is expected in the experimental conditions due its higher molecular weight. Thus, it is essential to promote a Lf residence time increase on the corneal surface and a penetration improvement into the stroma.

The novelty of this current work relies on challenging both chitosan-based formulations appropriateness for the enhancement of the drug corneal permanence and penetration, as well as assess the ability to sustain and control the drug release. These novel DDS are non-irritant to the ocular surface and produce an improved ocular retention time, thus providing greater efficacy and bioavailability. Additional advantages include: (I) high biocompatibility, (II) easiness of elaboration, (III) no need for high restrictions during the formulation procedure, high encapsulation and loading efficiencies, higher physical stability upon storage, and improved drug permeability.

Cyclodextrins can positively influence the protein stability, both thermally (temperature increase, ...) and chemically (inactivation by acids, ...). Furthermore, cyclodextrins can chemically interact with aromatic amino acids and promote the formation of inclusion complexes. SBE- -CD, a -CD derivative, can also stabilize proteins, not only by the formation of inclusion complexes, but also by electrostatic interaction phenomena (16). Moreover, this cyclodextrin can act as a complexing agent in the formation of chitosan nanocarriers by ion gelation technique, being able to act as an alternative substitute to the TPP. In addition, it has also been described the role of this cyclodextrin in terms of penetration and adhesion phenomena to corneal and scleral tissue.

Likewise, the main purpose for this site-specific and controlled release strategy is mainly based on the achievement of an improved pharmacokinetic and pharmacodynamic drug profile, as well as a better immunogenicity and system recognition for an enhanced therapeutic efficacy.

The aim of this work was based on the design, preparation, and characterization of lactoferrin-loaded CS/TPP and CS/SBE- -CD nanoparticles as topical ophthalmic drug delivery systems as a pharmacological alternative for keratoconus treatment. A comparison between the traditional CS/TPP nanoparticles and CS/SBE- -CD nanoparticles in order to carry out the immobilization of high molecular weight proteins intended for topical ophthalmic administration.

An effort to demonstrate the suitability of both chitosan-based formulations to control the lactoferrin delivery and enhance the corneal permeability was also carried out by obtaining a consistent preclinical base, not just through *in vitro* tests, but also with *ex vivo* and *in vivo* assays. Certainly, a novel ocular biopermanence study of polymeric nanoparticles based on a radiolabeling technique with different radiotracers were carried out to assess the bioadhesion of particles intended for ophthalmic topical administration.

MATERIALS

Low molecular weight chitosan (LMWCS; Mw = 150 kDa, 85% deacetylation degree and 85% purity grade) and pentasodium tripolyphosphate (TPP) were purchased from Sigma-Aldrich (St Louis, USA). Glacial acetic acid, sodium hydroxide (NaOH) and hydrochloric acid (HCl) were acquired from Merck (Darmstadt, Germany). Sulfobutylether-β-cyclodextrin (SBE- -CD; Mw = 2160 Da, substitution degree = 3.00 – 6.50) was provided by Cyclolab Ltd (Budapest, Hungary). Lactoferrin was acquired from Sigma-Aldrich (St Louis, USA). Type II porcine mucin was purchased from Sigma Chemical Co (St Louis, USA). Visking® dialysis tubing cellulose membrane (14,000 g/mole molecular weight cut-off) was purchased from Sigma Aldrich (St. Louis, Missouri, USA). Ultrapure water (Milli-Q®, Millipore Iberica, Madrid, Spain) was used throughout the entire work. All other chemicals and reagents were of the highest purity grade commercially available.

EXPERIMENTAL METHODS

Screening study: CS/TPP and CS/SBE- -CD nanoparticles formation. Chitosan-based nanoparticles were prepared by ionotropic gelation. This technique is based in the electrostatic interaction of chitosan amino groups (positively charged) with the TPP (17) or SBE- -CD (18) groups (negatively charged). Preliminary experiments were carried out before the drug encapsulation process to determine the best ratio between components that enable the nanoparticle's formation.

Preparation of blank CS/TPP nanoparticles. A 0.2% (w/v) chitosan solution was prepared by dissolving LMWCS in a 1% (v/v) acetic acid aqueous solution under stirring (500 rpm) for 24 h at room temperature. Dilutions were made in Milli-Q® water to the final desired concentrations. The pH was then adjusted to 5 (pH 5) with a 1M NaOH aqueous solution and stored in refrigeration (4 ± 2°C) until use. A tripolyphosphate (TPP) aqueous solution was prepared by dissolving the salt in Milli-Q® water to a final concentration of 0.2% (w/v) under stirring (500 rpm) for 24 h at room temperature and then stored in refrigeration (4 ± 2°C) until use. All TPP and chitosan solutions were filtered through a 0.22 µm PVDF membrane (Merck Millipore Durapore™) prior to storage.

CS/TPP nanoparticle's formation occurred by the addition of the TPP solution to the chitosan solution drop-wisely (v = 10 mL/min) at a 5:1 (v/v) CS:TPP ratio under vigorous magnetic stirring (> 750 rpm) at room temperature for 30 min in order to promote nanoparticle's gelation (17). TPP final concentrations in the preparation varied from 0.05% to 0.2% (w/v), while CS final concentrations follow the same pattern, from 0.05% to 0.2% (w/v).

Resulting CS/TPP nanoparticle's suspensions were centrifuged for 1 h at 14000 rpm at 25°C and the obtained sediment was resuspended in double-distilled water, analyzed and finally lyophilized, using 10% (w/v) trehalose as cryoprotectant. Dried particles were re-dispersed in a specific ocular buffer (pH 7.4) and characterized in terms of size, surface charge and morphology.

Preparation of blank CS/SBE- -CD nanoparticles. Chitosan and SBE- -CD solutions were prepared by dissolution in Milli-Q® water. A 0.2% (w/v) chitosan aqueous solution was prepared by dissolving LMWCS in a 1% (v/v) acetic acid aqueous solution under stirring (500 rpm) for 24 h at room temperature, filtered through a 0.22 µm PVDF membrane (Merck Millipore Durapore™) and pH was subsequently adjusted to 5 (pH 5) with a 1M NaOH aqueous solution and stored in refrigeration (4 ± 2°C) until use. The SBE- -CD solutions were prepared by jointly dissolving the cyclodextrin in desired concentrations into Milli-Q® water under stirring for 24 h at room temperature.

CS/SBE- -CD nanoparticle's formation occurred by the addition of the SBE- -CD solution to the chitosan solution drop-wisely (v = 10 mL/min) at a 5:1 (v/v) CS:SBE- -CD ratio under vigorous magnetic stirring (> 750 rpm) at room temperature for 30 min, allowing the system's complete stabilization. SBE- -CD final concentrations in the preparation varied from 0.1% to 0.5% (w/v), while CS final concentrations range from 0.025% to 0.1% (w/v).

Resulting CS/SBE- -CD nanoparticle's suspensions were centrifuged for 1 h at 14000 rpm and 25°C, and the sediment was then resuspended in double-distilled water, analyzed and subsequently lyophilized, using 10% (w/v) trehalose as cryoprotectant. Dried particles were re-dispersed in a specific ocular buffer (pH 7.4) and characterized in terms of size, surface charge and morphology.

Preparation of lactoferrin-loaded CS/TPP nanoparticles. Lactoferrin-loaded CS/TPP nanoparticles were prepared by the addition of predetermined amounts of protein (from 0.1 to 1.0 mg/mL) to the TPP aqueous solution under magnetic stirring (> 750 rpm), prior to the nanoparticle's formation by the ionotropic gelation technique, as previously described (see *Preparation of blank CS/TPP nanoparticles*). The lactoferrin was added to the TPP solution due to the protein's isoelectric point (Ip = 7.28), where TPP aqueous solution showed a pH 9, as a way to keep the protein's isoelectric balance during the elaboration process.

Resulting lactoferrin-loaded CS/TPP nanoparticle's suspensions were centrifuged for 1 h at 14000 rpm at 25°C and the obtained sediment was resuspended in double-distilled water, analyzed and lyophilized, using 10% (w/v) trehalose as cryoprotectant. Dried particles were re-dispersed in a specific ocular buffer (pH 7.4) and characterized in terms of size, surface charge and morphology. The supernatant was recovered for further analysis.

Preparation of lactoferrin-loaded CS/SBE- -CD nanoparticles. Predetermined amounts of lactoferrin (from 0.1 to 1 mg/mL) were incubated under magnetic stirring (500 rpm, 1 h) in a SBE-β-CD solution to promote the inclusion complex formation. These inclusion-complexed solutions were then used for nanoparticle's formation by the ionotropic gelation technique, as previously described (see *Preparation of blank CS/SBE- -CD nanoparticles*).

Resulting lactoferrin-loaded CS/SBE- -CD nanoparticle's suspensions were centrifuged for 1 h at 14000 rpm at 25°C and the obtained sediment was resuspended in double-distilled water, analyzed and lyophilized, using 10% (w/v) trehalose as cryoprotectant. Dried particles were re-dispersed in a specific ocular buffer (pH 7.4) and characterized in terms of size, surface charge and morphology. The supernatant was recovered for further analysis.

Physicochemical characterization of chitosan-based nanoparticles.

Particle size, size distribution and potential. The average particle size, polydispersity index (PDI) and potential of the chitosan-based nanoparticles were assessed by dynamic light scattering (DLS) with non-invasive back dispersion at 25°C, using a Malvern Zetasizer Nano ZS instrument (ZEN3600, Malvern Instruments Ltd., Malvern, UK). A 1:10 dilution in purified water was applied to samples before measurement in order to reduce the opalescence during size analysis and subsequently placed in disposable polystyrene cuvettes (DTS1070, Malvern Instruments Ltd., Malvern, UK) for the analysis. Each batch was analyzed in triplicate. DLS subsets were defined as presented: (I) 120 seconds temperature stabilization time for each sample, (II) 3 analysis runs for each formulation, and (III) 20 determinations per run for each sample.

Morphological evaluation. The morphological examination of the CS/TPP and CS/SBE- -CD nanoparticles was performed by scanning electron microscopy (SEM) and transmission electron microscopy (TEM). SEM analysis were performed by placing the samples on a metal stub double-sided conductive adhesive tape and iridium sputter-coating the samples prior to observation in an analytical scanning electron microscope (ZEISS EVO LS 15/EDX, ZEISS®) (Jena, Germany), under different magnifications. TEM analysis was performed by staining samples with 2% (w/v) phosphotungstic acid for 10 min, placed on copper grids with Formvar® film and dried overnight for TEM observation by using a JEOL JEM-F200CF-HR microscope (JEOL®) (Peabody, USA). The air-dried batches were imaged using a 200 kV acceleration power.

Production yield (PY) of nanoparticles. The PY (%) of the colloidal systems was acquired by the application of the centrifugation technique (19), with minor modifications. Briefly, predefined volumes of the NPs suspensions were centrifuged without glycerol bed (14000 rpm, 1h, 25°C), the supernatants were then discarded, and the sediment was vacuum-dried for 48h at 50 ± 2°C (until constant weight). The PY (%) was then estimated by comparing the final weight with the NPs theoretical weight, as presented:

Production yield (%) = (Nanoparticles weight)/(Total initial solids weight)·100

Encapsulation efficiency (EE) and loading capacity (LC) of nanoparticles. EE (%) and LC (%) of the resulting formulations were acquired after isolation by centrifugation, as previously described. EE denotes the entrapped drug (%) from the total amount of drug initially added to the preparation, while LC refers to the percentage of encapsulated drug into the NPs. The amount of unbound lactoferrin was determined in the supernatant by UV-Vis spectrophotometry (Cary 60 UV-Vis, Agilent Technologies®) (California, USA) at a 280 nm wavelength. The EE and LC of lactoferrin were respectively calculated as presented below:

EE (%) = (Total amount of drug - Amount of unbound drug)/(Total amount of drug)·100

LC (%) = (Total amount of drug - Amount of unbound drug)/(Nanoparticles weight)·100

Stability studies. The NPs aggregation or contraction phenomena are expected to be influenced by the drug physicochemical properties. Additionally, chemical processes, including oxidation or hydrolysis, may also alter the useful lifespan of chitosan-based nanoparticle suspensions. The stability of chitosan-based nanoparticles should be assessed in terms of structural changes, such as contraction and swelling processes, among others (20).

Stability to storage. The stability study during storage was designed as per ICH guidelines (21), with minor modifications. Selected nanoparticle's formulations were freshly prepared, isolated by centrifugation and resuspended in a specific ocular buffer (pH 7.4), considering size changes and possible precipitation phenomena. Nanoparticles were incubated at three different temperature conditions: (I) in refrigeration (4 ± 2°C), (II) at room temperature (25 ± 2°C), and (III) oven temperature (37 ± 2°C) for a 8 h (short-time stability) and 3-month (long-term stability) period respectively, under orbital agitation (100 rpm) sheltered from the light. Samples were collected at predetermined time points for both studies. Nanoparticle's size and size distribution were measured by DLS, performing every measurement in triplicate.

Stability to pH. The pH-dependent nanoparticle's physical stability evaluation was carried out in freshly prepared samples. Once obtained and after a three-times Milli-Q® water washing, suspensions were kept in refrigeration at 4 ± 2°C as stock suspensions. 500 µL of each formulation were taken to test tubes and diluted to a 5 ml volume using Milli-Q® water. pH was then adjusted to predetermined values (2, 4, 6, 7, 8, 10 and 12) by using 0.1M NaOH or 0.1M HCl aqueous solutions, as appropriate. Samples were kept in refrigeration at 4 ± 2°C for 24 h, followed by the particle size, PDI and potential measurements. Each sample was measured in triplicate.

Stability to ionic strength. NPs physical stability assessment in terms of ionic strength was performed in freshly prepared samples. Once obtained and after a three-times Milli-Q® water washing, suspensions were kept in refrigeration at 4 ± 2°C as stock suspensions. 500 µL of each formulation were taken to test tubes and diluted to a 5 ml volume using NaCl aqueous solutions with predetermined molarity values (0.2, 0.4, 0.6, 0.8, 1.2, 1.4, 1.6 and 2M). Samples were kept in refrigeration at 4 ± 2°C for 24 h, followed by the particle size, PDI and potential measurements. Each formulation was tested and measured in triplicate.

***In vitro* release study**. The dialysis technique is one of the most versatile and widespread used to assess drug delivery from nanosized DDS. In this method, two different chambers are physically separated by the usage of a dialysis membrane. Several modifications have subsequently been applied in crucial factors as a way to improve the experimental process (22). Furthermore, the ease of the system and sampling procedure make it an appropriate, simple, and uncomplicated technique to assess the drug delivery profile from a wide-ranging variety of nano-sized DDS (23).

The Lf release from CS/TPP and CS/SBE- -CD NPs was assessed to predict the drug diffusion and pharmacokinetic behavior from the DDS in simulated physiological conditions. The osmolality of formulations was adjusted to better replicate the topical ophthalmic administration. Hence, freshly prepared lactoferrin-loaded CS/TPP and CS/SBE- -CD nanoparticles were suspended in PBS (pH 7.4 and ionic strength 0.075 M) due to the fact that the buffer osmolality is in the optimal range (from 0.025 to 0.15 M) for a physiological environment proof-of-concept assay and characterization in terms of drug delivery (24).

The lactoferrin release rate from CS/TPP and CS/SBE- -CD nanoparticles was determined by UV-Visible spectrophotometry (Cary 60 UV-Vis, Agilent Technologies®) (California, USA), using Franz diffusion cells. The receptor chamber was fully filled with 7 mL of phosphate buffer medium (PBS, pH 7.4) containing 0.02% (w/v) sodium azide, while donor chamber was filled 3 ml of a known amount of lactoferrin-loaded nanoparticles. Both chambers were separated by a Visking® dialysis membrane. Sink conditions were established in order to simulate *in vivo* pharmacokinetic behavior.

Franz diffusion cells were subsequently placed in an orbital shaker bath (Unimax 1010/Incubator 1000, Heidolph®) (Schwabach, Germany) which was kept at 37°C and under magnetic stirring (100 rpm). At predetermined time points, 1 ml was taken from the receptor chamber, and refilled with an equivalent volume of fresh PBS solution in order to maintain sink conditions. The study was run for 24 h, and each formulation was tested in triplicate.

Lactoferrin concentrations in the pH 7.4 isotonic PBS solution were measured using UV-Vis spectrophotometry (Cary 60 UV-Vis, Agilent Technologies®) (California, USA) at a 280.0 nm wavelength. Resulting data demonstrated that reference solutions remained stable for at least a week, protected from light exposure and under refrigeration (4 ± 2°C).

Cytotoxicity analysis. The accomplishment in designing, developing and certifying alternative trials to replace the Draize rabbit eye irritation test has remained indefinable due to the difficulty of comparing *in vitro* resulting data with the in vivo data obtained from the animal models (robustness and consistency), but some tests have shown considerable

potential for the evaluation of ocular irritancy. Organotypic models have risen as the most promising alternative approaches to the eye irritation assessment, including isolated eyes or components thereof, among others (25). The effectiveness of these *in vitro* and *ex vivo* procedures is well established within different regulatory societies and industry for explicit and restricted determinations.

The Bovine Corneal Opacity and Permeability test (BCOP) is appropriate to evaluate the DDS harshness into the ocular surface, where injury depth can be estimated in an *ex vivo* tissue model. Nevertheless, the BCOP resolution for minor ocular cytotoxicity grades is deficient. Hence, BCOP can be considered as a pre-validation assay and it is suggested to be used in tandem with other assays measuring different cytotoxicity endpoints, such as the Hen's egg test on the chorioallantoic membrane assay (HETCAM), among others (26). On its behalf, the chorioallantoic membrane (CAM) of the fertilized chicken eggs is also considered an appropriate model for assessing the effects of DDS on the eye tissue, being able to detect even mild or very mild ocular irritant compounds.

Bovine Corneal Opacity and Permeability test (BCOP). The BCOP test is an organotypic assay used to assess the potential cytotoxicity of formulations, avoiding the keeping and killing of laboratory animals (animal replacement compliance).

The use of *in situ* isolated corneas have the advantage that all corneal layers can be assessed, from the epithelium to the endothelium. Furthermore, tests on isolated corneas generally involve simple techniques with accurate measurable endpoints.

The use of BCOP assay is based on the method developed by Tchao et al. (1988) (27) and adapted by Gautheron et al. (28), with minor modifications. Briefly, freshly excised eyes were collected from a local slaughterhouse and transported in superfusion containers that enable their maintenance for the desired period, enough for the formulation's testing in the laboratory. The eyes were then inspected by macroscopic analysis and the corneas, free of defects, were dissected and used as the test systems.

Freshly isolated corneas were vertically mounted in Franz diffusion cells, used as holders, with the corneal epithelial surface upwards. The mounted corneas divided the diffusion cell into two different chambers (donor and receptor, respectively). All Franz diffusion cells were incubated in a thermostatic bath with controlled temperature (37 ± 2°C) and under magnetic stirring (100 rpm) during the entire assay.

In the BCOP test, corneal opacity changes were assessed by the onset of two different techniques, these being the luxmetry and the UV-Vis spectrophotometry. Luxmetry is assessed by placing the dissected cornea inside a specially designed luxmeter (Gossen Mavolux 5032C USB) (Nürnberg, Germany). On the other hand, UV-Vis spectrophotometry is determined by transmittance scan (from 200 to 800 nm), positioning the cornea in an specific holder in order to allow the light to pass through, from the source to the receiver of the spectrophotometer (Cary 60 UV-Vis, Agilent Technologies®) (California, USA). Each formulation was evaluated in triplicate.

A procedure for formulation's addition and opacity measurements was established as presented: (I) determination of the initial opacity values for freshly excised corneas by luxmetry and UV-Vis spectrophotometry; a corneal blank was made before luxmetry determination in order to remove basal light, while the cornea itself was used as blank (at a 800 nm wavelength) before spectrophotometry determination, (II) addition of 1 mL PBS into the Franz cell's donor compartment and cornea's incubation for 10 minutes, followed by the opacity determination, (III) 1 mL of the formulation is added to the upper chamber (enfolding the corneal epithelium) for 10 minutes, followed by its removal and subsequent addition of PBS for 120 minutes; after this time, the opacity determination is repeated.

Likewise, after measuring the opacity, 1 mL of the 0.4% (w/v) fluorescein aqueous solution was added to the epithelium side to evaluate the corneal permeability by assessment of the media optical density (OD) (PBS) in the receptor chamber at a 490 nm wavelength, as a way to assess corneal permeability changes.

The opacity and permeability measurements were used to calculate the *in vitro* irritation score (IVIS) (28). Furthermore, classification of test formulations can be done according to the Kay and Calandra score (28). The mathematical equation used for the IVIS determination is presented as:

IVIS = mean opacity value + (15 × mean permeability OD_{490} value)

Hen's egg test on the chorioallantoic membrane (HET-CAM). The HET-CAM cytotoxicity assay for the assessment of irritant substances is based on the Draize test (1944) (29) and has become one of the most widely used international standard assay for ocular irritation evaluation (OECD TG 405, 2002; EC B.5). However, different validated alternative tests (animal replacement) showed considerable promise for ocular irritancy evaluation. The HET-CAM assay is a new organotypic model that enables the identification of cytotoxic compounds, similarly to the Draize test procedure (30).

In the HET-CAM assay, three outcomes are measured, these being: (I) hemorrhage, (II) lysis and (III) coagulation of the chorioallantoic membrane at the 9th day of embryonation, when nervous system and pain sensitivity have not been developed yet. These reactions can be quantified through an irritation score (IS) and subsequently classified as follows: (I) 0-0.9 as no irritation, (II) 1-4.9 as slight irritation, (III) 5-8.9 as moderate irritation and (IV) 9-21 as severe irritation, following the Kalweit et al. criteria (31). All HET-CAM procedures were applied following the handling of animal materials frameworks.

The protocol used was adapted from the procedure previously described by Spielmann and Liebsch (32). Briefly, fertilized Broiler eggs (50 – 60 g weight) were obtained from the regional hatchery technology center and incubated for nine days in specific conditions (37 ± 0.5°C and 65% ± 5% RH). The trays containing eggs were automatically rotated in every 2 h until eighth day, where rotation was stopped, and the eggs were maintained in the axial position for the proper placement of the CAM.

At ninth day of incubation, viable embryos were used by creating a window on the head of the eggs through which formulations (300 µL) were instilled. After placing the formulation onto the CAM, an assessment of the aforementioned factors over a 5 min period was performed by using an Olympus SZ61TR Stereomicroscope and an Olympus CellSens Entry software. Images were taken at the beginning (before formulation's administration) and at the end (after the trial period) of the assay and each replicate was recorded during the entire process in order to carefully assess the presence or absence of toxic effects (if required). These measurements were individually studied, and subsequently combined to obtain a final score, which was used to categorize the irritation grade of each formulation. A 0.9% (w/v) NaCl aqueous solution was used as negative control, while a 1M NaOH aqueous solution was employed as positive control. Each formulation was evaluated in triplicate.

Mucoadhesion study. The interaction between chitosan and mucin defines the chitosan-based DDS behavior. Interactions between chitosan and mucin are related to intrinsic factors (polymer nature) and external factors (environment where the interaction occurs). The interrelationship between both types of factors must be taken into account. Thus, four different outcomes could be observed as a result of the interaction between chitosan-based nanoparticles and the ocular mucin layer (see Figure S-1, Supporting Information): (I) adsorption of the nanoparticles to the mucus layer, (II) nanoparticle's removal with the mucus layer renewal, (III) loss of functionality of the nanoparticles when covered by mucin, or (IV) passage through the mucin layer and reach the cornea.

Accordingly, the mucoadhesive properties of chitosan-based DDS should be deeply studied. Two different approaches were used to assess the ocular retention time of the formulations after topical ophthalmic administration into the eye, as presented: (I) *in vitro* ocular retention study by biophysical techniques (potential measurements), (II) *ex vivo* ocular retention study by using excised bovine eyes, and (III) *in vivo* ocular retention study by using male Sprague-Dawley rats as animal model.

***In vitro* ocular mucoadhesion study**. The *in vitro* ocular surface retention study was based on a mucoadhesion assay procedure, considering the electrostatic interaction between the chitosan amino groups (positive charge) and mucin structure (negative charge) (33).

Experimentally, mucoadhesion study was performed following the procedure described by Mazzarino et al. (34), with minor modifications. Equal volumes of 0.4 mg/mL mucin solution and CS/TPP or CS/SBE- -CD nanoparticles were vortexed for 1 min and furtherly kept in an orbital incubator (37 ± 2°C, 100 rpm) for 2 h. Chitosan/mucin interactions were then stopped by maintaining the nanoparticle's suspensions on an ice bath (2 - 8°C) for 45 min and the potential of the resulting mixtures was subsequently measured. It must be taken into account that nanoparticle's potential was measured before and after the incubation process with the mucin solution, and the mucoadhesion ability was measured as the difference between both values.

***Ex vivo* ocular mucoadhesion study**. The *ex vivo* corneal surface retention study was adapted from the original procedure described by Belgamwar et al, (2009) (35), with minor modifications. For this purpose, freshly excised eyes were collected from a local abattoir and transported in superfusion containers that allow their maintenance for a specified time period, enough for the formulation's testing in the laboratory. The eyes were then inspected by macroscopic analysis and viable ones were selected for further analysis.

Viable excised eyes were washed with PBS (pH 7.4) in order to remove possible impurities and then placed on manually developed specific holders, positioning the corneal epithelial surface upwards. 500 µL of the 0.4% (w/v) fluorescein-stained chitosan-based nanoparticles were added drop wisely, and excess was collected and reapplied, repeating this procedure 10 times. The final residual solution was measured for fluorescence intensity by UV- Vis spectrophotometry (Cary 60 UV-Vis, Agilent Technologies®) (California, USA) at a 490.0 nm wavelength, comparing it to the initial intensity values, obtained by measuring the suspension prior to the instillation.

The *ex vivo* corneal mucoadhesion of the CS/TPP and CS/SBE- -CD nanoparticles was subsequently quantified through the following mathematical equation:

$$\text{Mucoadhesion (\%)} = ((Abs_0 - V_0) - ((Abs_F - V_F))/((Abs_0 - V_0))\cdot 100$$

Where Abs_0 and Abs_F represent the absorbance value for the initial and final fluorescein-stained chitosan-based suspensions, V_0 refers to the volume applied to the viable excised eyes, and V_F indicates the final volume of the suspension not adsorbed to the mucosa. Each formulation was tested in triplicate.

***In vivo* mucoadhesion study**.

Evaluation of the radiolabeling stability and efficiency of chitosan-based nanoparticles. Radioactive fluoride (^{18}F) is one of the most frequently applied positron emitters due to its optimal positron characteristics ($t_{1/2}$ = 109.7 min), making it almost ideal for Positron Emission Tomography (PET) imaging. In spite of all these advantages, ^{18}F is mostly clinically applied into two different forms, these being 2-[^{18}F]fluoro-2-deoxy-D-glucose (^{18}F-FDG) and ^{18}F-Choline.

Recently, different approaches were studied to track different types of colloidal systems using ^{18}F-FDG or ^{18}F-Choline labeling (36,37). Based on this literature review, the assessment of the radiolabeling stability and efficiency of ^{18}F-FDG or ^{18}F-Choline chitosan-based nanoparticles was carried out by incubation with a known amount of the radiotracer for a 45 min period at 25 ± 2ºC, and under magnetic stirring (200 rpm) (ThermoCell® Mixing Block, Tamar Laboratory Supplies Ltd., Israel). Samples were then centrifuged at predetermined times (0.5, 1.5 and 3.0 h) (14000 rpm and 4ºC) (Eppendorf® 5427R, Eppendorf Iberica, Spain), supernatant and remnant were separated into two different centrifuge tubes, and radiotracer activity was finally measured by using an activimeter (Capintec® CRC 15R Dose Calibrator, New Jersey, USA). In order to point out, both types of the ^{18}F-based aqueous solution (^{18}F-FDG and ^{18}F-Choline) were provided by the PET Radiopharmaceutical Unit (Cyclotron) of the University Hospital Complex of Santiago de Compostela (CHUS).

The radiolabeling efficiency of chitosan-based nanoparticles was assessed by measuring the ^{18}F-FDG or ^{18}F-Choline activity respectively, both in the supernatant and the remnant vials, taking into account the incubation time and the radiotracer decay. Mathematical analysis was then performed to the resulting data to obtain the radiolabeling efficiency and to assess the labeling stability over time.

Experimental *in vivo* evaluation of the ocular biopermanence. The *in vivo* assessment of the ocular surface retention time of the formulations was carried out by Positron Emission Tomography (PET) and Computed Tomography (CT) combined technique. Both methodologies for leading the radiolabeling and the subsequent measurable ocular surface permanence evaluation of topical ophthalmic formulations were described in previous works (38).

In vivo studies were performed on male Sprague-Dawley rats (250 ± 35 g), supplied by the animal facility at the Center for Experimental Biomedicine (CEBEGA, USC, Spain). The animals were maintained in individual enclosures under predetermined temperature (22 ± 1ºC) and relative humidity (60 ± 5%) conditions, with circadian cycles (12/12 hours) controlled by artificial light and *fed ad libitum*. Animals were familiarized for 7-day period prior to the experiment's commencement. All animals were preserved according to the Association for Research in Vision and Ophthalmology Statement (ARVO), as well as the official laboratory standards for animal experimentation (39). Each formulation was tested in quadruplicate (four eyes, two animals) in order to accomplish the 3Rs regulatory frameworks (40).

The microPET and CT acquisition was performed by using the Albira PET/CT Preclinical Imaging System (Bruker Biospin, Woodbridge, Connecticut, United States). Sedated animals were placed into the PET/CT bed with a muzzle mask (2.5% (v/v) isoflurane/oxygen), monitoring the breathing frequency during the achievement period. Then, 7.5 µL of ^{18}F-FDG radiolabeled chitosan-based nanoparticles were instilled into the ocular surface. After the instillation, static PET frames at predetermined times (0, 30, 75, 120, 240 and 300 minutes) were acquired in order to estimate the pharmacokinetic behavior. An Elizabethan collar was placed in each animal between PET studies to prevent the rat from scratching their eyes and removing the previously instilled formulation.

Imaging reconstruction (0.5 x 0.5 x 0.5 mm^3 pixel size) was carried out by using the maximum likelihood expectation maximization algorithm (MLEM) (6 iterations). Image analysis was made using the specific software (41). Regions of Interest (ROIs) were manually acquired and processed after imaging reconstruction for the different frames over time by delimiting the total radiotracer's uptake of each eye (15 x 15 x 15 mm, 1767.10 mm^3), and the resulting data were adjusted by the radiotracer's radioactive decay (half-life time: 109.7 min). Results were repeated on consecutive predefined time frames. The radiotracer uptake (mean ± SD) acquired from the first time-point after topical ophthalmic administration of the formulations was considered as the fitting factor. The subsequent measurements from the successive time-points were described as percentage of the fitting factor. Resulting graphs of formulation's radioactivity vs time were subsequently made, comparing the results against a control solution (^{18}F-FDG buffered solution).

The adjustment of the retained formulation over time to a mono-exponential decay equation using a single compartmental model was carried out by non-lineal regression using the GraphPad Prism® software (42). Non-compartmental analysis was also carried out by estimating the mean residence time (MRT) and the total area under the curve (AUC) of the remaining percentage of formulations over time.

Data analysis. A pairs of groups comparison was performed by a one-tailed Student's T and multiple group comparison tests, as well as by one-way or two-way analysis of variance (one-way or two-way ANOVA), or by non-parametric Kruskal Wallis test with a 95% significance level ($p < 0.05$) throughout these studies, using the GraphPad Prism v.8.00 software (GraphPad Software, Inc. CA, USA). All data were shown as a mean value and its standard deviation (mean ± SD). Tukey's, Bonferroni's or Dunnet's tests were subsequently applied for post-hoc contrast.

RESULTS AND DISCUSSION

Screening study: CS/TPP and CS/SBE- -CD nanoparticles formation.

Preparation of CS/TPP nanoparticles. CS/TPP NPs were prepared via the ionotropic gelation technique, based on the ionic interaction between CS and TPP, leading to the formation of inter- and intramolecular connections (17). The ion gelation method was mild, and a few minutes were taken to create the final nanoparticles.

CS/TPP NPs preparation was carried out in acidic conditions due to the fact that the pH of the medium influenced the protonation of the CS amino groups (pH interval = 5 - 6). Pilot studies were focused to the selection of the optimal proportion for the CS/TPP nanoparticle's formation. The presence of opalescence in the resulting solutions was used as a signal of NPs formation, subsequently confirmed by DLS.

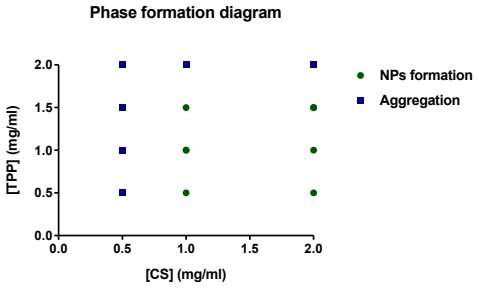

Figure 1. Phase diagram formation of CS/TPP NPs.

The increase in the turbidity of the suspensions (CS/TPP NPs formation) was directly proportional to the amount of TPP used, but particle aggregation rapidly and drastically occurred (see Figure 1). Higher available amount of TPP led to the formation of larger nanoparticles and flocculating aggregates as a consequence of dominantly inter- and intramolecular cross-links. All the suspensions prepared in the selected interval of TPP and CS concentrations were deeply analyzed in terms of particle size, size distribution and surface charge (see Figure S-2, Supporting Information).

The preliminary results of these preparations indicate that a 1:1 (w/w) CS/TPP ratio and a 5:1 (v/v) phase ratio turned out to be the best proportion for CS/TPP nanoparticle's formation.

Preparation of CS/SBE- -CD nanoparticles. The ratio between CS and SBE- -CD is a critical parameter in the nanoparticle's formation and restricts the resulting particle size. Hence, it was essential to estimate the best CS/SBE- -CD ratio to promote the best conditions for the formation of the nanosystems before the drug encapsulation. Different concentrations of CS and SBE- -CD were used to establish the optimum preparation conditions for nanoparticle's formation. The CS/SBE- -CD NPs preparation was carried out in acidic conditions since the pH of the medium influenced the protonation of the CS amino groups (pH 5).

In the present study, SBE- -CD was incorporated into final formulations to improve drug stability, water solubility, encapsulation efficiency and release profile into the nanocarriers. Carried-out studies have shown that all NPs were in the nano-sized interval and showed a positive potential. Likewise, the phase diagram of nanoparticle formation (see Figure 2) reveals the existence of an interval with different specific ratios of SBE- -CD and CS in order to make nanoparticle's formation possible. Two different systems were identified in the phase diagram, including (I) opalescent dispersion and (II) aggregates (see Figure 2) for the tested concentration interval.

The increase in the turbidity of the suspensions (CS/SBE- -CD NPs formation) was directly proportional to the amount of SBE- -CD used, but particle aggregation promptly and significantly occurred (see Figure 2). Higher available amount

of SBE- -CD led to the formation of larger nanoparticles or flocculating aggregates as a consequence of dominantly inter- and intramolecular interactions between both components. All the suspensions were deeply analyzed in terms of particle size, size distribution and surface charge (see Figure S-3, Supporting Information).

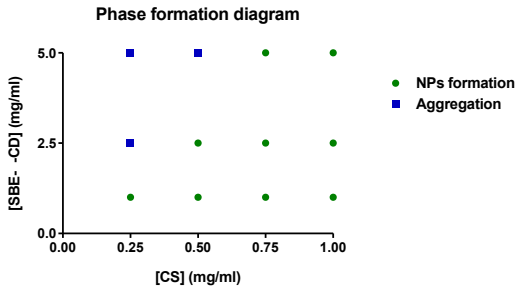

Figure 2. Phase diagram formation of CS/SBE- -CD NPs.

Based on the resulting data, an optimum CS/SBE- -CD ratio was selected for the preparation of lactoferrin-loaded NPs, these being composed of 0.05% (w/v) chitosan and 0.25% (w/v) SBE- -CD solutions in a 5:1 (v/v) phase ratio.

Physicochemical characterization of nanoparticles.

Particle size, size distribution and potential. Particle size and size distribution of novel nanoparticulate systems are important factors considering their potential purpose for topical ophthalmic administration. Indeed, it is well known that particles in the nanometric range influence biological parameters, such as the *in vivo* distribution through biological barriers, drug delivery to the target tissue, drug content, stability or toxicity, among others (43).

Preliminary results of CS/TPP nanoparticles indicate that a 5:1 (v/v) CS/TPP ratio turned out to be the best proportion for nanoparticle's formation. The average size was 160.56 ± 20.65 nm. The polydispersity index (PDI) was lower than 0.3 for the chosen CS/TPP ratio (about 0.170 ± 0.067), indicating that a homogeneous dispersion was obtained. The distribution curve suggests the presence of two different particle size populations: a small fraction of 1000 nm (< 2%) (nanoparticle aggregates) and a major population of around 150 nm (> 98%) (nanoparticles). Nevertheless, during the elaboration procedure, nanoparticle's suspensions were filtered through a 0.45 µm PVDF membrane filter in order to remove the larger aggregates. Regarding the surface charge, compact complexes were spontaneously formed due to the interaction between CS and TPP; hence, final formulations were measured by DLS, obtaining high positively potential values (16.13 ± 1.67 mV) (see Table 1) due to the CS presence in the surface (44). This positively charged is required to prevent particle aggregation phenomena and promote electrostatic interaction with the negatively-charged cell phospholipidic bilayer (45).

On its behalf, CS/SBE- -CD nanoparticles were developed under the assumption that these systems could be prepared in the absence of TPP, by only mixing CS with different amounts of SBE- -CD, a negatively charged CD derivative, which could be more effectively incorporated into nanoparticles as a consequence of strong ionic interactions with the amino groups of the CS. The average size was 227.3 ± 20.52 nm. The polydispersity index (PDI) was found to be smaller than 0.3 (0.182 ± 0.07), indicating a relative homogeneity in the resulting formulation. The potential studies of the nanoparticles showed high positive values (about 17.2 ± 1.25 mV), revealing that the NPs surface was mostly composed of CS (see Table 1).

Table 1. Physicochemical characterization for blank and lactoferrin-loaded chitosan-based nanoparticles.

Formulation	[Lactoferrin] (mg/mL)	Size (nm)	PDI	ζ Potential (mV)
Blank CS/TPP NPs	-	160.56 ± 20.56	0.170 ± 0.067	16.13 ± 1.67
Blank CS/SBE- -CD NPs	-	227.3 ± 20.52	0.182 ± 0.070	17.2 ± 1.25
Lactoferrin-loaded CS/TPP NPs	0.1	125.59 ± 10.01	0.244 ± 0.050	9.42 ± 0.76
	0.5	166.46 ± 42.27	0.287 ± 0.040	9.41 ± 1.90

	1.0	150.48 ± 13.44	0.294 ± 0.150	8.69 ± 1.36
Lactoferrin-loaded CS/SBE- -CD NPs	0.1	221.83 ± 9.48	0.220 ± 0.038	15.53 ± 1.55
	0.5	242.01 ± 20.26	0.266 ± 0.040	16.62 ± 3.10
	1.0	196.07 ± 3.02	0.213 ± 0.014	14.54 ± 2.49

*Each measurement was carried out in triplicate (n = 3)

Morphological evaluation. SEM images were examined to demonstrate that the nanoparticle's size was kept after the freeze-drying process. SEM analysis after the freeze-drying process confirmed the presence of monodisperse population of spherical in shape and irregular surface particles with size below 300 nm, although some aggregation phenomena due to the drying process was observed (see Figure S-4, Supporting Information). Thus, the freeze-dried formulations guarantee the nanoscale size, where the microstructural analysis confirmed the morphology and size of the nanoparticles. These results were aligned with TEM morphological evaluation for both types of nanoparticles.

The TEM images provide information about the particle size and morphology of nanoparticles, as well as confirm previous DLS measurements. The microstructural analysis confirmed that both types of nanoparticles are presented as a predominantly monodisperse population of isolated and spherical particles with well-defined solid and consistent structure (see Figure 3).

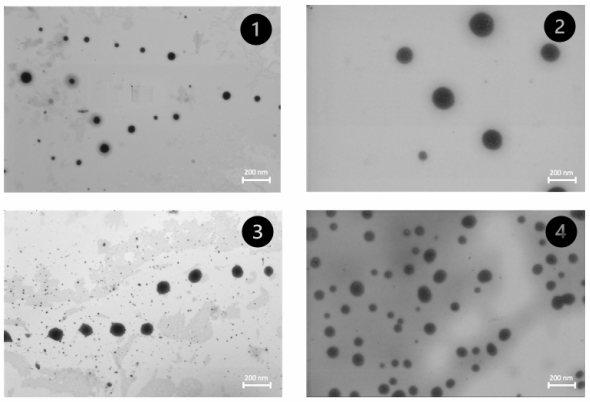

Figure 3. TEM images of chitosan-based nanoparticles (CS/TPP NPs – 1 and 2 - and CS/SBE- -CD NPs – 3 and 4 -, respectively). Images 1, 3 and 4 were obtained with a 5.00 kX magnification, while image 2 was obtained with a 15.00 kX magnification, in order to better appreciate CS/TPP nanoparticle morphology.

A diameter interval of 103.7 ± 13.2 nm (CS/TPP NPs) and 185.0 ± 12.1 nm (CS/SBE- -CD NPs) was obtained for the resulting nanoparticulate systems based on the TEM micrographs, smaller than the diameter determined by DLS. This could have been expected since the nanoparticles were dispersed in an aqueous phase for DLS analysis (CS swelling in water), while the TEM trials were performed in dry samples (46).

Production yield, encapsulation efficiency and loading capacity of nanoparticles. Two different chitosan-based nanosystems were developed for protein encapsulation. It is known that chitosan acidic solutions (pH 5) may interact with the negatively charged polyanions, such as TPP or SBE- -CD, ionic cross-linkages, leading to the formation of chitosan-based nanoparticles (47).

Table 2 shows the production yield (PY), encapsulation efficiency (EE) and loading capacity (LC) values of the resulting lactoferrin-loaded CS/TPP and CS/SBE- -CD nanoparticles. The encapsulation efficiency determination demonstrated that the elaboration process of lactoferrin-loaded CS/TPP and CS/SBE- -CD nanoparticles was reproducible and efficient with production yield values above 31.53 ± 3.94% and 24.00 ± 2.69%, respectively (see Table 2). It must be considered that the drug:polymer ratio in this study ranged from 1:1 to 1:1.4. A directly proportional increase in the EE and LC values was observed with the increase in the amount of drug added into the formulation (e.g., 5:1 or 10:1 ratios). A two-way ANOVA analysis was applied to the resulting data in order to determine the existence of differences between CS/TPP and CS/SBE- -CD nanoparticles. The results indicate that there were no significant differences in

terms of PY, and between formulations with the same Lf concentration in terms of EE and LC, but significant differences ($p < 0.05$) were observed between increasing Lf-concentration formulations in terms of EE and LC.

Effect of protein loading on size, surface charge, EE (%) and LC (%). Lactoferrin, which shows an isoelectric point (Ip) around 7.28 (48), was directly added to the anionic solution (pH 9, where the protein would be positively charged) and then TPP or SBE- -CD aqueous solutions were added drop wisely. As shown in Table 2, the presence of the model protein has a small influence on particle size. In order to point out, potential values of both lactoferrin-loaded CS/TPP and CS/SBE-β-CD NPs were lower than blank formulations (see Table 2), suggesting that the protein could not be just encapsulated inside the nanosystems, but also attached to the nanoparticle's external shell, partly masking the CS's inherent positive charges. This finding is supported by the study carried out by Tantra el al. (49), where it is suggested that NPs external charges are influenced by the molecular organization of all the compounds at the NPs shell and the net constituted by the chemical positions.

Likewise, visual analysis of the resulting data (see Figure 4) seems to indicate that an increased in the EE and LC values is observed by increasing the amount of lactoferrin added to the formulation, but without significant modifications in size. A two-way ANOVA analysis confirmed this hypothesis, where statistically significant differences ($p < 0.05$) were observed for both types of nanoparticles in terms of EE (%) and LC (%), but not in terms of size ($p > 0.05$). Thus, an increase in the initial amount of lactoferrin could improve EE and LC values in this kind of chitosan-based nanosystems.

A Dunnet's multiple comparisons test was also applied to assess the existence or absence of statistically significant differences in terms of size. No differences were observed for both types of formulations ($p > 0.05$). Similarly, a Tukey's multiple comparisons test was applied to evaluate the existence or absence of statistically significant differences in terms of EE (%) and LC (%), where statistically noteworthy variances were detected for both chitosan-based nanosystems ($p < 0.0001$) over the increased amount of incorporated lactoferrin.

Stability studies.

Stability to storage. The short-term stability determination of CS/TPP and CS/SBE- -CD nanoparticles was performed by determining the size, size distribution and surface charge by keeping samples at three different temperature sets (4 ± 2°C, 25 ± 2°C/60 ± 5% RH and 37 ± 2°C/60 ± 5% RH) for 8 h, while the long-term stability study was carried out under the same conditions but for a 3-month period.

Previous studies have also shown the CDs role in the nanoparticle's stabilization. Certainly, -CD derivatives have been widely used to improve the aqueous solubility and the chemical stability of different active substances, by forming host−guest complexes. This complexation process usually leads to a modulation of the drug physicochemical properties of the guest molecule (i.e., solubility, ocular penetration, or stability) (50).

Table 2. PY, EE and LC values for chitosan-based nanoparticles.

Formulation	[Lf] (mg/ml)	Size (nm)	PY (%)	EE (%)	LC (%)
Blank CS/TPP NPs	-	130 ± 20.65	84.39 ± 2.65	-	-
Blank CS/SBE- -CD NPs	-	227.28 ± 20.52	85.80 ± 3.42	-	-
Lf-loaded CS/TPP NPs	0.1	135.59 ± 10.01	85.89 ± 4.96	24.78 ± 3.60	12.39 ± 1.80
	0.5	146.46 ± 22.27	84.13 ± 2.96	34.85 ± 2.24	26.14 ± 1.68
	1.0	150.48 ± 13.44	84.19 ± 2.67	47.19 ± 2.97	43.47 ± 5.04
Lf-loaded CS/SBE- -CD NPs	0.1	221.83 ± 19.48	83.86 ± 2.02	20.49 ± 6.00	11.18 ± 3.27
	0.5	242.01 ± 20.26	85.37 ± 3.51	38.67 ± 1.01	30.26 ± 0.79
	1.0	215.51 ± 18.77	84.91 ± 2.95	52.84 ± 1.05	43.44 ± 3.69

*Each measurement was carried out in triplicate (n = 3)

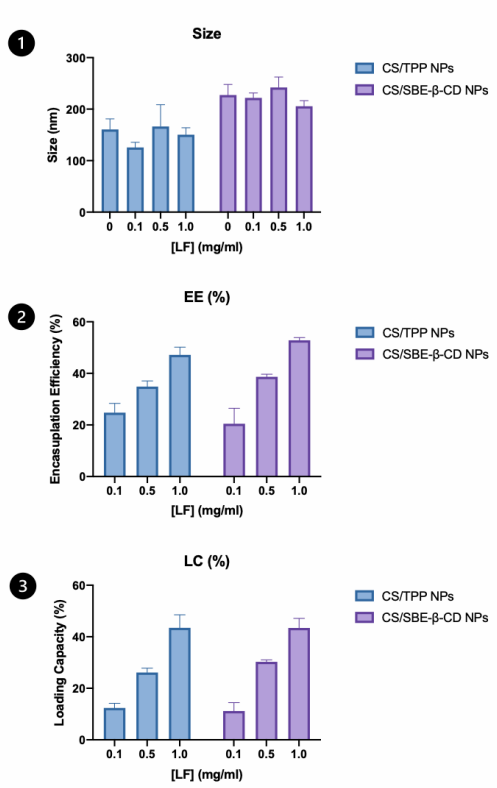

Figure 4. (1) Evolution of size (nm) over increased lactoferrin concentration for CS/TPP and CS/SBE- -CD nanoparticles. PDI values were under 0.3 (from 0.194 to 0.244 for CS/TPP NPs, and from 0.213 to 0.287 for CS/SBE- -CD NPs), associated with a uniform and monodisperse population. (2) EE (%) values over increased lactoferrin concentration for CS/TPP and CS/SBE- -CD nanoparticles. (3) LC (%) values over increased lactoferrin concentration for CS/TPP and CS/SBE- -CD nanoparticles.

The results for the short-term stability study showed that both formulations (CS/TPP and CS/SBE- -CD nanoparticles) did not suffer a significant change in their size following incubation for 8 h (data not shown, included into the long-term stability study; see Figure S-5, Supporting Information). Same results were observed for long-term stability over a 3-month period (see Figure 5).

Resulting data were analyzed and no changes in size were observed during the studied period, where size varied within an interval of less than 10% of the initial average size. A two-way ANOVA analysis was also applied, and no statistically significant differences ($p < 0.05$) were observed for the studied period. Thus, it can be concluded that both types of nanoparticles are stable over time.

Stability to pH. Changes in the pH conditions of the media may be generally associated with nanoparticle's collapse, breakage, or coalescence phenomena. Figure 6 shows particle size and potential changes of CS/TPP and CS/ SBE- -CD nanoparticles for the tested pH interval.

A transition from positive to negative potential values was gradually observed with increasing pH values. Nevertheless, no particle size changes were observed from pH 2 to 7, while aggregation phenomenon appears in basic pH range (up to pH 8). In order to point out, although topical ophthalmic formulations should have a pH value similar to the tear film (pH 7), the presence of salts, proteins and others ocular substances, provides the ocular surface a buffering ability, increasing the pH interval that can be tolerated by the eye without causing ocular surface damages or tearing (pH interval: from 4 to 8) (51); hence, these formulations could be safely applied into the eye by topical ophthalmic administration.

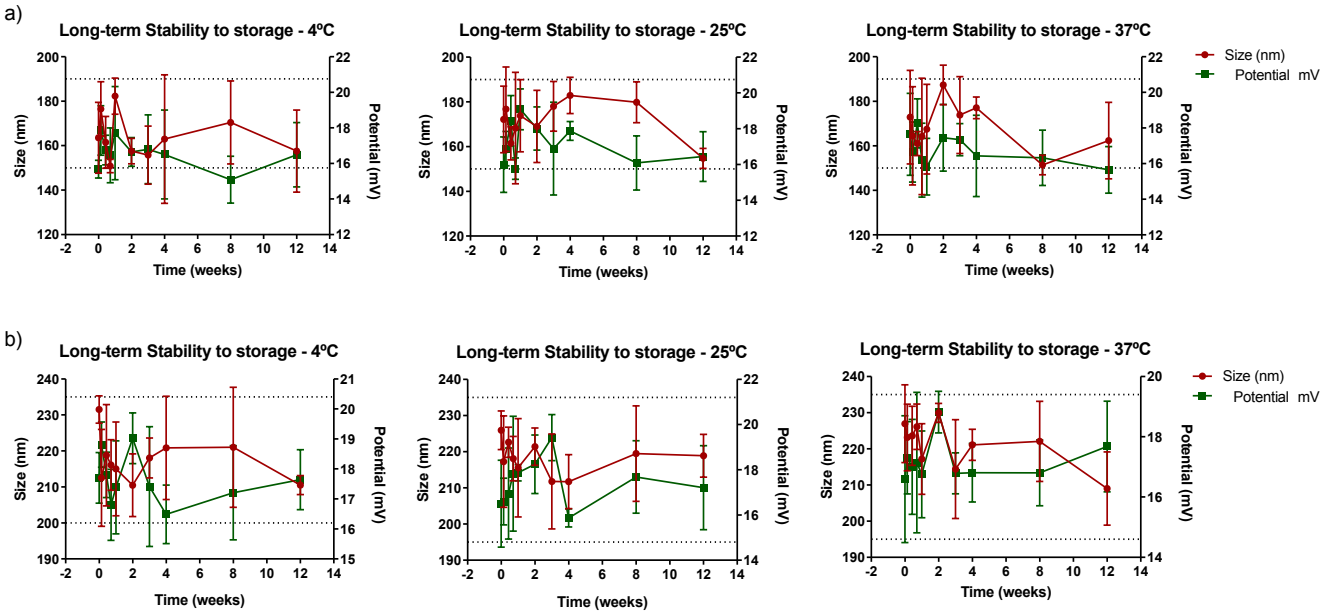

Figure 5. Long-term stability-to-storage study for CS/TPP and CS/SBE- -CD NPs ("a)" and "b)", respectively) over a 3-month period. Stripped lines show the 10% variation size interval from the initial mean size values, which comprises the nanoparticle stability range.

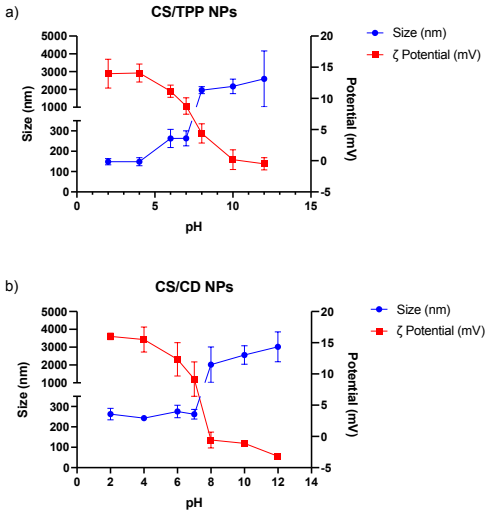

Figure 6. Changes in size and potential values of CS/TPP (a) and CS/SBE- -CD (b) NPs over the studied pH interval.

Stability to ionic strength. Changes in the ionic strength conditions of the media may be generally associated with nanoparticle's collapse, breakage, or coalescence phenomena. This statement is supported by the DLVO theory, which explains a decrease in the thickness of the diffuse bilayer with accumulative ionic strength values (52). Thus, an increase in the particle-particle interaction leads to a rise in the nanoparticle's aggregation phenomenon.

The physical stability to ionic strength depends on possible time-dependent aggregation, flocculation or sedimentation phenomena of the nanoparticles (53). Changes in the particle compactness over time may also influence either of these processes. Figure 7 shows the resulting data for the stability-to-ionic-strength study of CS/TPP and CS/SBE- -CD NPs for the ionic strength tested interval.

Both CS/TPP and CS/SBE- -CD NPs were in the nanometric size range for normal values of ionic strength in an ocular medium (from 0.075 to 0.15M). The colloidal stability of CS/TPP nanoparticles was kept constant regardless of the increased ionic strength conditions of the media, although a ζ potential lowering was observed with the increasing salt concentration of the media. Indeed, as observed in Figure 7, CS/TPP formulations stored in the presence of NaCl were mostly stable in terms of size, turbidity, and particle compression changes over the time period studied.

Nevertheless, a coalescence process was observed in the CS/SBE- -CD NPs with increasing amounts of NaCl in the media. This phenomenon suggests that electrostatic repulsion is the predominant stabilization mechanism for this type of formulation. Aggregation process may be associated with the high concentration of monovalent ions (mainly Na^+) of the cyclodextrin formulation (135 mOsm/kg, see SBE- -CD technical sheet specifications), which in turn contributes to an increase in the final nanoparticle formulation osmolality. Even so, the CS/SBE- -CD NPs remained stable over the normal ionic strength interval (0.075M to 0.15M), making them appropriate DDS for topical ophthalmic administration.

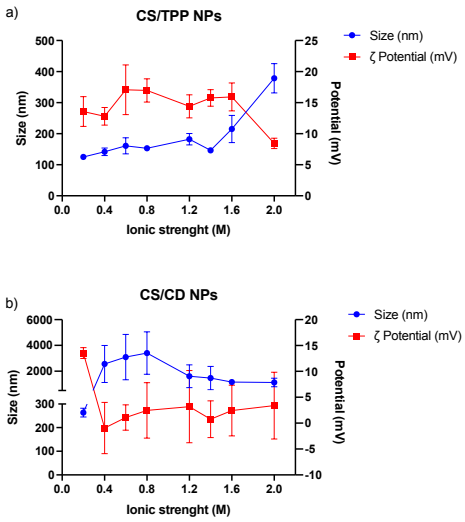

Figure 7. Changes in size and potential values of CS/TPP (a) and CS/SBE- -CD (b) NPs over the ionic strength studied interval.

***In vitro* release study**. The preliminary *in vitro* release study from lactoferrin-loaded CS/TPP and CS/SBE- -CD nanoparticles proves that both formulations present a sustained release pattern, compared to the control solution (Lf buffer solution) as shown in Figure 8. The *in vitro* protein release profiles obtained for each formulation showed two different release phases, as follows: (I) a first initial burst release due to the drug desorbed from the NPs surface and (II) a plateau release phase, resulting from the protein diffusion from the polymer matrix as a consequence of bioerosion processes.

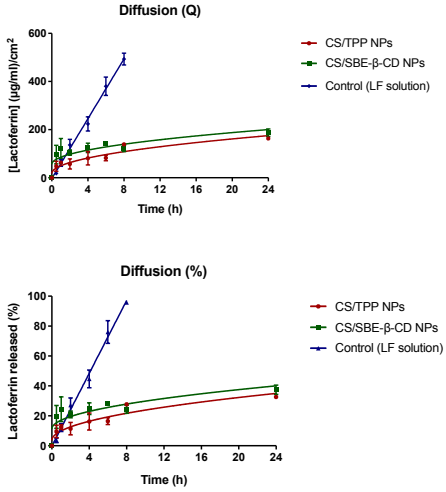

Figure 8. *In vitro* release study of CS/TPP and CS/SBE- -CD NPs. The first graph shows the raw cumulative amount of lactoferrin released over time (h), while the second graph presents the cumulative percentage of lactoferrin released over time (h).

The resulting data from lactoferrin cumulative release from CS/TPP and CS/SBE- -CD NPs were fitted to two different kinetic models (Higuchi and Peppas and Korsmeyer) in order to identify the release mechanism. The best correlation data was obtained with the Higuchi kinetic model, suggesting that diffusion was the main release mechanism (see details in Table 3).

Table 3. Release data of chitosan-based nanoparticles into the Higuchi diffusion kinetics and Peppas and Korsmeyer equation.

Formulation	Higuchi		Peppas and Korsmeyer		
	k ($g \cdot cm^{-2} \cdot min^{-0.5}$)	R^2	k ($g \cdot cm^{-2} \cdot min^{-n}$)	n	R^2
CS/TPP NPs	32.13	0.8663	52.50	0.3585	0.8451
CS/SBE- -CD NPs	29.42	0.8245	102.7	0.1614	0.8211

Cytotoxicity analysis.

Bovine Corneal Opacity and Permeability test (BCOP). Endpoints measured during the BCOP test for both types of formulations were assessed in terms of opacity (light transmission through the cornea by luxmetry and UV-Vis spectrophotometry) and permeability (fluorescein passage through the entire corneal tissue).

Firstly, opacity and permeability values were independently studied to evaluate whether formulations induce corrosivity or severe irritation (see Figure S-6, Supporting Information). Resulting data indicate that no significant structural changes were observed in terms of corneal opacity and fluorescein permeability, comparing them with the negative control solution (PBS and ethanol as negative and positive control solutions, respectively) (see Figure 9).

Likewise, opacity and permeability data were corrected for background or control values prior to further statistical determinations were calculated. The IVIS score was then calculated by combination of both types of empirically derived values for each formulation. Both formulations (CS/TPP and CS/SBE- -CD NPs) resulted in an *in vitro* Irritation Score of 0 (IVIS = 0), showing no cytotoxicity effects compared to control formulations (see Figure 9).

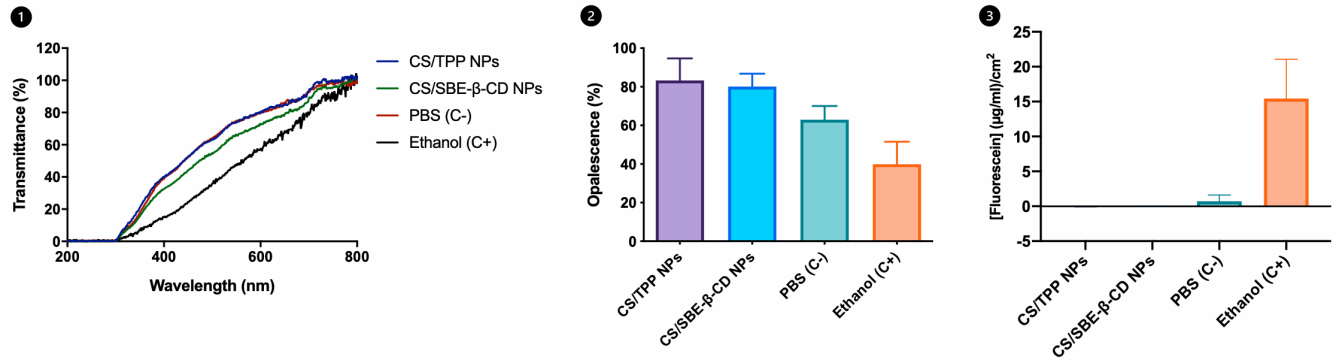

Figure 9. BCOP results for chitosan-based nanoparticles. (1) Resulting data of corneal transparency for both chitosan-based nanoparticles, compared to the results of the control solutions. (2) Opalescence data of corneal tissue after the administration

of chitosan-based formulations, compared to control values. (III) Fluorescein corneal permeability for CS/TPP and CS/SBE- -CD nanoparticles compared to the control solution results.

Hen's egg test on the chorioallantoic membrane (HET-CAM). The CAM is a no innervated tissue and constitutes a well-developed vascularization model and an easy-to-study alternative strategy for ocular irritation assessment due to the broad inflammatory process response, similar to that induced in the Draize test, as it can be carried out with better effectiveness and faster determinations than other *in vivo* assays (54). Thus, the HET-CAM assay was used to assess the cytotoxicity and biocompatibility of prepared nanoparticles.

CS/TPP and CS/SBE- -CD nanoparticles were evaluated, and the resulting data were compared with those obtained for the BSS and NaOH solutions, used as negative and positive control formulations, respectively. All formulations show no cytotoxicity effects (Irritation Score = 0), comparing them with both control formulations (see Figure S-7, Supporting Information). This is in good agreement with previously published works (55), as well as in accordance with the results of the BCOP test, confirming that the materials used and the developed nanosystems are non-toxic and biocompatible.

Ocular surface mucoadhesion study.

***In vitro* mucoadhesion study**. Ocular mucus layer is a heterogeneous three-dimensional network composed of a mucin fiber's network where nanoparticles may diffuse through and/or be retained (56,57). Hence, the mucus layer can affect the stability of CS/TPP and CS/SBE- -CD nanoparticles (58). Chitosan is a mucoadhesive polymer that may increase the residence time of the formulation, consequently improving the drug bioavailability (59). In this study, the interaction between mucin and CS/TPP and CS/SBE- -CD nanoparticles was determined by DLS (60), evaluating the size and potential changes before and after the nanoparticle/mucin interaction (61).

Figure 10 shows the size and potential values for CS/TPP and CS/SBE- -CD nanoparticles, before and after the incubation in mucins suspensions. The increased size after the incubation procedure suggests that the interaction between mucin and CS/TPP or CS/SBE- -CD nanoparticles led to the formation of nanoaggregates and a decrease in potential values, probably due to the electrostatic interaction between chitosan and mucin (61). Furthermore, a strong ability of CS/TPP and CS/SBE- -CD nanoparticles to interact with mucin through electrostatic forces was proved, emphasizing their potential as mucoadhesive DDS (34).

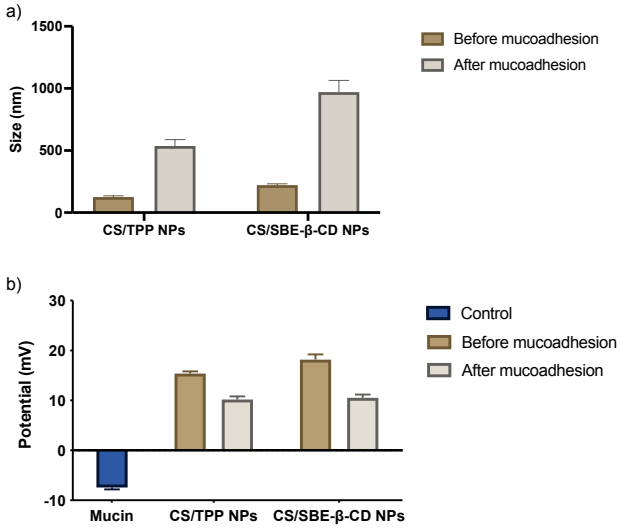

Figure 10. Changes in size (a) and potential (b) values for chitosan-based nanoparticles during the *in vitro* ocular surface retention study.

***Ex vivo* corneal surface mucoadhesion study**. Mucin layer in the corneal surface is a key factor that must be considered in the design and development of pharmaceutical forms intended for the topical ophthalmic administration. Figure 11 shows the mucoadhesion variation for both types of chitosan-based nanoparticles in terms of the difference in the fluorescein concentration before and after the *ex vivo* ocular surface retention study.

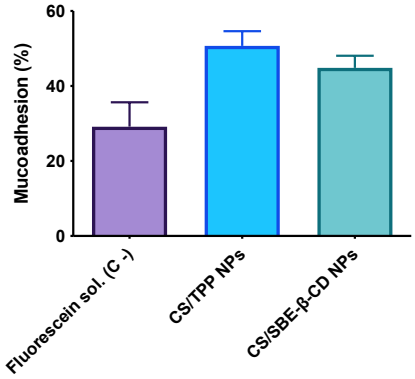

Figure 11. Mucoadhesion values (%) for chitosan-based nanoparticles during the *ex vivo* ocular surface retention study.

It was found that mucoadhesive properties of chitosan-based formulations were greater in the *in vitro* studies than *ex vivo* studies. This may be since formulations were instilled in a single administration during the *ex vivo* study, reducing the contact time between the formulation and the mucin layer, compared to the *in vitro* ocular surface retention study, where formulations were kept in contact with the mucin solution for a predetermined time. Thus, a reduction in the mucoadhesive strength of nanoparticles is observed.

In addition, a one-way ANOVA analysis was applied and statistically significant differences ($p < 0.05$) were observed by comparing the resulting data obtained for both formulations with the control fluorescein solution.

***In vivo* ocular surface permanence study**.

Evaluation of the radiolabeling stability and efficiency of chitosan-based nanoparticles. Figure S-8 (Supporting Information) shows the ^{18}F-FDG or ^{18}F-Choline radiolabeling stability and efficiency for chitosan-based nanoparticles, respectively. As presented, ^{18}F-FDG chitosan-based nanoparticles showed a high radiolabeling efficiency (up to 70%) and great stability along the studied period (up to 3h), while ^{18}F-Choline radiolabeling efficiency was lower (around 20%) but maintaining stability over time.

It must be taken into account that ^{18}F-Choline radiolabeling efficiency increased over time (from 10 to 25%), possibly due to the fact that more incubation time is needed for the radiolabeling process to take place. Based on these results, ^{18}F-FDG was selected as the radiotracer for further *in vivo* radiolabeling assays.

Experimental *in vivo* evaluation of the residence time on the ocular surface. Figure 12 shows the ^{18}F-FDG-radiolabeled chitosan-based ocular biopermanence along the studied interval, compared to a control solution (^{18}F-FDG aqueous buffered solution, pH 7.4). The ocular permanence of the both chitosan-based nanoparticles was characterized on male rats by ^{18}F-FDG radiolabeling, followed by the radioactivity assessment in a microPET system over a 5 h (300 min) period. It is a useful and non-invasive technique employed in the determination of the pharmacokinetic profiles of topical ophthalmic DDS (38,62,63).

In the present study, a higher residence time was observed for both types of nanoparticles, compared to the control solution, despite the fact that all formulations show a composition close to the tears. The resulting data was properly fitted to a monoexponential decay profile using a single compartmental model (R^2 = 0.9813 for CS/TPP NPs, R^2 = 0.9935 for CS/SBE- -CD NPs, and R^2 = 0.9930 for ^{18}F-FDG control solution) (see Figure 12). These results support the idea that both formulations exhibit good mucoadhesive, headline penetration and, presumably, direct cell uptake properties, and are in good agreement with the PET data described in previous studies (39-41).

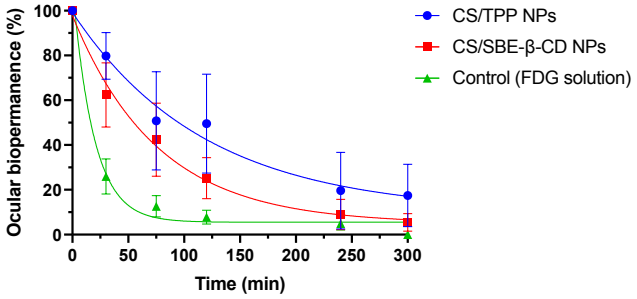

Figure 12. ^{18}F-FDG radiolabeled chitosan-based NPs clearance ratio (%) from the ocular surface determined by PET, compared to a control solution (^{18}F-FDG buffered aqueous solution). Ocular biopermanence (%) remaining on the ocular surface over time was calculated assuming initial biopermanence value (%) recorded in the ROI.

Table 4 shows the pharmacokinetics parameters ($t_{1/2}$, MRT, and k) of the ^{18}F-FDG radiolabeled chitosan-based nanoparticles and ^{18}F-FDG control formulations. Statistically significant differences ($p < 0.05$) were observed between both types of formulation compared to the control solution in terms of diffusion coefficient (k, min^{-1}) and half-life time ($t_{1/2}$, min), but no differences between both chitosan-based nanoparticle formulations. Similar behavior was also observed for MRT, AUC and % dose 30 min parameters.

Both types of nanoparticles show greater biopermanence than the control formulation (see Figure 13). However, the apparent lower ocular permanence of the CS/SBE- -CD NPs observed in the monoexponential decay curve shown in Figure 12 may be associated with their more sensitivity to the presence of salts in the tear film that produces a decrease of the NP surface charge with a possible increase in the aggregation phenomena, causing a slight decrease in the adherence to the corneal mucous layer.

Table 4. Release data of chitosan-based nanoparticles into the diffusion

Formulation	K (min^{-1})		$t_{1/2}$ (min)		MRT (min)		AUC		% dose 30 min	
	Mean	SD	Mean	SD	Mean	SD	Mean	SD	Mean	SD
CS/TPP NPs	0.008	0.005	114.4	72.0	127.3	47.1	17114	9874.0	79.8	10.5
CS/SBE- -CD NPs	0.013	0.005	60.5	20.1	89.9	13.7	9316	2553.7	62.4	14.3
^{18}F-FDG Control solution	0.041	0.012	17.7	4.5	59.1	17.6	4131	919.9	26.0	7.8

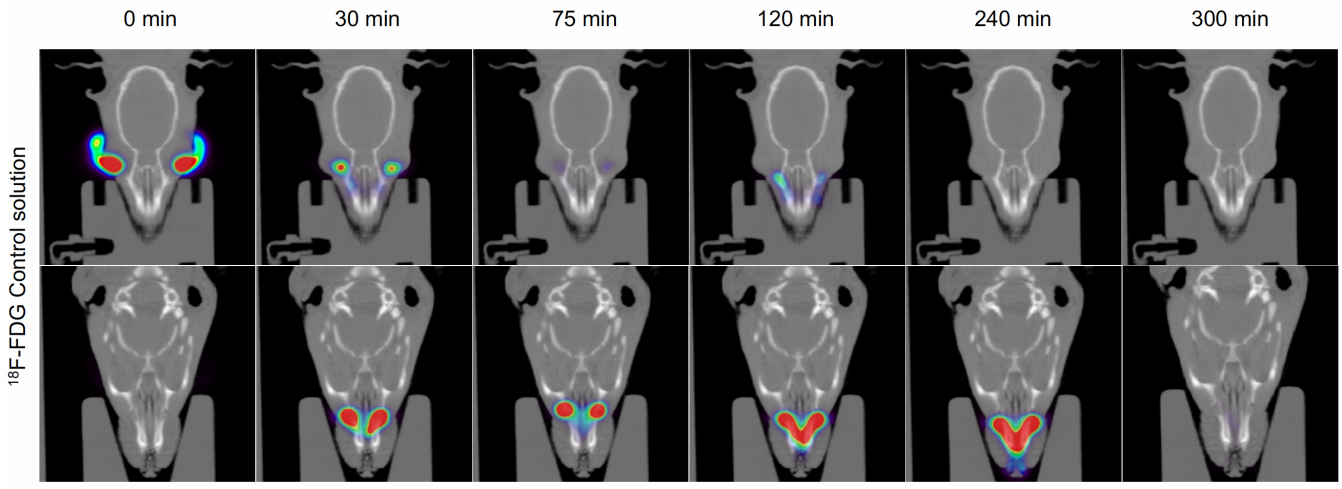

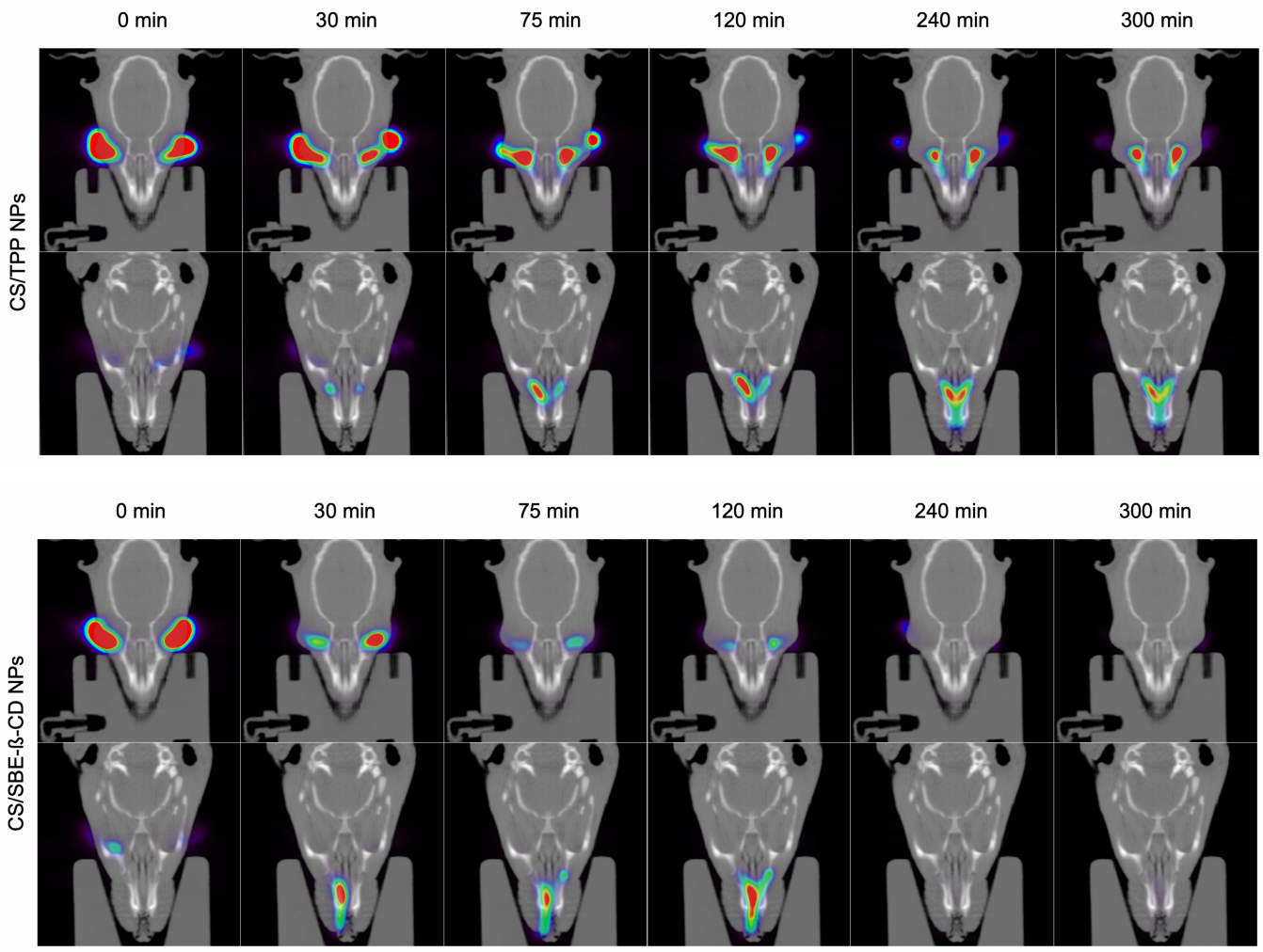

Figure 13. Fused PET/CT images displayed in coronal plane representing rat's eye and nasolacrimal duct at different time points (0, 30, 75, 120, 240 and 300 min) post-administration.

CONCLUSION

The preparation of CS/TPP and CS/SBE- -CD nanoparticles by ionotropic gelation is highly sensitive to different environmental parameters, as well as preparation procedure conditions. The elaboration process of both types of nanoparticles involves several critical parameters, including the optimization of chitosan's, TPP's or SBE- -CD's concentration, pH and ionic strength of the media or CS/TPP or CS/SBE- -CD ratio, among others, in order to obtain stable nanoparticles of tunable size and charge (64,65).

In the present work, low molecular weight chitosan with highest degree of deacetylation was selected and novel ionic crosslinked nanoparticles composed of CS/TPP and CS/SBE- -CD loaded with lactoferrin were successfully prepared. An average particle size of 160.56 ± 20.65 nm and 227.3 ± 20.52 nm, as well as a surface potential of 16.13 ± 1.67 mV and 17.2 ± 1.25 mV were obtained for CS/TPP and CS/SBE- -CD nanoparticles, respectively. Both formulations were spherical in shape and irregular surface particles with size below 300 nm.

Similarly, both formulations show good stability to storage for, at least, three months, as well as no particle size changes were observed from pH 2 to 7 interval and were in the nanometric size range for normal values of ionic strength in an ocular medium (from 0.075 to 0.15M). A controlled release of lactoferrin was also achieved from the both types of nanoparticles, confirming their use as potential drug delivery systems for protein drugs.

Results also demonstrated mucoadhesive nanoparticles without relevant cytotoxicity. A strong ability of CS/TPP and CS/SBE- -CD nanoparticles to interact with mucin through electrostatic forces was observed, showing a higher ocular retention profile for, at least, 240 min.

In conclusion, it is proposed, for the first time, two different chitosan-based formulations as biodegradable mucoadhesive nanocarriers for delivery of lactoferrin. This is supported by extensive *in vitro* and *in vivo* characterization studies. A preclinical consistent base was achieved for the first pharmacological treatment for keratoconus as an alternative to the current invasive clinical methods, since there are no therapeutic alternatives, only existing non-pharmacological (use of contact lenses or glasses) or surgical procedures as palliative or supportive treatment.

Analogously, both nanoparticles show appropriate physicochemical properties suitable for topical ophthalmic administration, supporting the idea that they are retained in the corneal layer, prolonging the drug release time from the tissue itself, something that may guarantee the patient's adherence to the treatment, since a lower dosage frequency would be required. Furthermore, the versatility of these systems would allow including them in different pharmaceutical forms for ophthalmic administration based on the requirements and characteristics of the patient, as a new way to partially personalize and individualize the therapeutic strategy. Nevertheless, a better correlation with *in vivo* data should be profoundly explored in order to deeply understand the real potential of these nanocarriers as a topical ophthalmic alternative strategy for the prevention and treatment of keratoconus.

ASSOCIATED CONTENT

Supporting Information

Additional materials of experimental methods and results.

The Supporting Information is available free of charge on the ACS Publications website.

Mucoadhesion study (PDF)
Screening study: Preparation of CS/TPP nanoparticles (PDF)
Screening study: Preparation of CS/SBE- -CD nanoparticles (PDF)
Morphological evaluation – SEM images (PDF)
Short-term stability-to-storage study (PDF)
Bovine Corneal Opacity and Permeability test (BCOP) (PDF)
Hen's egg test on the chorioallantoic membrane (HET-CAM) (PDF)
Evaluation of the radiolabeling stability and efficiency of chitosan-based nanoparticles (PDF)

AUTHOR INFORMATION

Corresponding Author

* Francisco Javier Otero Espinar: francisco.otero@usc.es
* María Isabel Lema Gesto: mariaisabel.lema@usc.es

Author Contributions

RVF contributed to the elaboration of the article and carried out the entire experimental analysis, as well as the writing original draft preparation. XGO gave support in the *in vivo* experimental part. VDT contributed in the cytotoxicity analysis. URL, MLL and MILG were responsible for the writing review and editing. MGB and FJOE were in charge of the conceptualization, funding acquisition and supervision of the project, as well as writing review and editing. All authors have given approval to the final version of the manuscript.

Funding Sources

RVF and XGO acknowledg**e** the financial support of the FIDIS (Health Research Institute of Santiago de Compostela Foundation). Similarly, URL and MLL recognize the support from Xunta de Galicia (Galician Innovation Agency GAIN: IN607A2018/3) and Spanish Research Network on Cerebrovascular Diseases INVICTUS PLUS (RD16/0019) fellowships.

This project has been awarded grant from the Spanish Ministry of Economy and Competitiveness (Instituto de Salud Carlos III: PI18/00159), and partially supported by the Spanish Ministry of Science, Innovation and Universities (RTI2018-099597-B-100).

ACKNOWLEDGMENT

SEM and TEM analysis were feasible thanks to the Electronic and Confocal Microscopy Unit of the Universidade de Santiago de Compostela (USC) (CACTUS, Spain).

ABBREVIATIONS

DDS, drug delivery system; CD, cyclodextrin; CS, chitosan; GlcN; 2-amino-2-deoxy-glucopyranose; GlcNAc; 2-acetamido-2-deoxy-β-D-glucopyranose; TPP, pentasodium tripolyphospate; SBE- -CD; sulfobutylether-β-cyclodextrin; ICRS; implanting intracorneal ring segments; CXL, cross-linking; MMP-9, matrix-9 metalloprotease; ZAG, zinc-α2-glycoprotein; IGKC, immunoglobulin kappa chain; Lf, lactoferrin; TLR, Toll-like receptor; LMWCS, Low molecular weight chitosan; PDI, polydispersity index; DLS, dynamic light scattering; SEM, scanning electron microscopy; TEM, transmission electron

microscopy; PY, production yield; EE, encapsulation efficiency; LC, loading capacity; PBS, phosphate buffer saline; BCOP, Bovine Corneal Opacity and Permeability; HETCAM, Hen's egg test on the chorioallantoic membrane; CAM, chorioallantoic membrane; OD, optical density; IVIS, *in vitro* irritation score; ^{18}F-FDG, 2-[^{18}F]fluoro-2-deoxy-D-glucose; PET, Positron Emission Tomography; CT, Computed Tomography, MLEM, maximum likelihood expectation maximization algorithm; ROI, region of interest; MRT, mean residence time; AUC, area under the curve.

REFERENCES

1. Patel A, Cholkar K, Agrahari V, Mitra AK. Ocular drug delivery systems: An overview. World J Pharmacol. 2013;2(2):47–64.

2. Kammona O, Kiparissides C. Recent advances in nanocarrier-based mucosal delivery of biomolecules. J Control Release Off J Control Release Soc. 2012 Aug 10;161(3):781–94.

3. Trapani A, Garcia-Fuentes M, Alonso MJ. Novel drug nanocarriers combining hydrophilic cyclodextrins and chitosan. Nanotechnology. 2008 May 7;19(18):1851-01.

4. Kymes SM, Walline JJ, Zadnik K, Sterling J, Gordon MO, Collaborative Longitudinal Evaluation of Keratoconus Study Group. Changes in the quality-of-life of people with kerato-conus. Am J Ophthalmol. 2008 Apr;145(4):611–7.

5. Godefrooij DA, de Wit GA, Uiterwaal CS, Imhof SM, Wisse RPL. Age-specific Incidence and Prevalence of Keratoconus: A Nationwide Registration Study. Am J Ophthalmol. 2017 Mar;175:169–72.

6. Romero-Jiménez M, Santodomingo-Rubido J, Wolffsohn JS. Keratoconus: a review. Contact Lens Anterior Eye J Br Contact Lens Assoc. 2010 Aug;33(4):157–66.

7. Meiri Z, Keren S, Rosenblatt A, Sarig T, Shenhav L, Varssano D. Efficacy of Corneal Collagen Cross-Linking for the Treatment of Keratoconus: A Systematic Review and Meta-Analysis. Cornea. 2016 Mar;35(3):417–28.

8. Sharif R, Bak-Nielsen S, Hjortdal J, Karamichos D. Pathogenesis of Keratoconus: The intriguing therapeutic potential of Prolactin-inducible protein. Prog Retin Eye Res. 2018 Nov;67:150–67.

9. Lema I, Brea D, Rodríguez-González R, Díez-Feijoo E, Sobrino T. Proteomic analysis of the tear film in patients with keratoconus. Mol Vis. 2010 Oct 13;16:2055–61.

10. Hayashida K, Kaneko T, Takeuchi T, Shimizu H, Ando K, Harada E. Oral administration of lactoferrin inhibits inflammation and nociception in rat adjuvant-induced arthritis. J Vet Med Sci. 2004 Feb;66(2):149–54.

11. Pattamatta U, Willcox M, Stapleton F, Cole N, Garrett Q. Bovine lactoferrin stimulates human corneal epithelial alkali wound healing in vitro. Invest Ophthalmol Vis Sci. 2009 Apr;50(4):1636–43.

12. Flanagan JL, Willcox MDP. Role of lactoferrin in the tear film. Biochimie. 2009 Jan;91(1):35–43.

13. Sobrino T, Regueiro U, Malfeito M, Vieites-Prado A, Pérez-Mato M, Campos F, Lema I. Higher Expression of Toll-Like Receptors 2 and 4 in Blood Cells of Keratoconus Patiens. Sci Rep. 2017 Oct 11;7(1):1–7.

14. Gesto MIL, Sánchez JAC, Moreiras TS, Perez FC. Biomarkers for diagnosis and prognosis of corneal ectatic disorders.

15. Charalel RA, Engberg K, Noolandi J, Cochran JR, Frank C, Ta CN. Diffusion of protein through the human cornea. Ophthalmic Res. 2012;48(1):50-55.

16. Serno T, Geidobler R, Winter G. Protein stabilization by cyclodextrins in the liquid and dried state. Adv Drug Deliv Rev. 2011 Oct 1;63(13):1086–106.

17. Kawashima Y, Tetsuro H, Akihiro K, Hideo T, Shan Yang L. The effect of thickness and hardness of the coating film on the drug release of theophylline granules. Chem. Pharm Bull. 1985; 33:2469–2474.

18. Zhang P, Liu X, Hu W, Bai Y, Zhang L. Preparation and evaluation of naringenin-loaded sulfobutylether-β-cyclodextrin/chitosan nanoparticles for ocular drug delivery. Carbohydr Polym. 2016 20;149:224–30.

19. Jithan A, Madhavi K, Madhavi M, Prabhakar K. Preparation and characterization of albumin nanoparticles encapsulating curcumin intended for the treatment of breast cancer. Int J Pharm Invetig. 2011;1(2):119–25.

20. Morris G, Castile J, Smith A, Adams G, Harding SE. The effect of prolonged storage at different temperatures on the particle size distribution of tripolyphosphate (TPP)-chitosan nanoparticles. Carbohydr Polym. 2011 Apr;84(4):1430–4.

21. Q 1 A (R2) Stability Testing of new Drug Substances and Products. 2006;20.

22. Chidambaram N, Burgess DJ. A novel in vitro release method for submicron-sized dispersed systems. AAPS PharmSci. 1999 Aug 31;1(3):32–40.

23. Muthu MS, Singh S. Poly (D, L-lactide) nanosuspensions of risperidone for parenteral delivery: formulation and in-vitro evaluation. Curr Drug Deliv. 2009 Jan;6(1):62–8.

24. Orthner MP, Lin G, Avula M, Buetefisch S, Magda J, Rieth LW, Solzbacher F. Hydrogel based sensor arrays (2 × 2) with perforated piezoresistive diaphragms for metabolic monitoring (in vitro). Sens Actuators B Chem. 2010 Mar 19;145(2):807–16.

25. Chamberlain M, Gad SC, Gautheron P, Prinsen MK. IRAG working group 1. Organotypic models for the assessment/prediction of ocular irritation. Interagency Regulatory Alternatives Group. Food Chem Toxicol Int J Publ Br Ind Biol Res Assoc. 1997 Jan;35(1):23–37.

26. Loprieno N. Alternative Methodologies for the Safety Evaluation of Chemicals in the Cosmetic Industry. CRC Press; 2019. 233 p.

27. Salem H, Katz SA. Alternative Toxicological Methods. CRC Press; 2003. 618 p.

28. Eskes C, Bessou S, Bruner L, Curren R, Harbell J, Jones P, Kreiling R, Liebsch M, McNamee P, Pape W, Prinsen MK, Seidle T, Vanparys P, Worth A, Zuang V. 3.3. Eye Irritation. Alternatives to Laboratory Animals. 2005; 33, 47–81.

29. Wallig MA, Haschek WM, Rousseaux CG, Bolon B, editors. Chapter 22 - Special Senses. In: Fundamentals of Toxicologic Pathology (Third Edition) [Internet]. Academic Press; 2018 [cited 2020 Mar 21]. p. 673–747.

30. Luepke NP. Hen's egg chorioallantoic membrane test for irritation potential. Food Chem Toxicol Int J Publ Br Ind Biol Res Assoc. 1985 Feb;23(2):287–91.

31. Kalweit S, Besoke R, Gerner I, Spielmann H. A national vali-dation project of alternative methods to the Draize rabbit eye test. Toxicol Vitro Int J Publ Assoc BIBRA. 1990;4(4–5):702–6.

32. Spielmann H, Kalweit S, Liebsch M, Wirnsberger T, Gerner I, Bertram-Neis E, Krauser K, Kreiling R, Miltenburger HG, Pape W, Steiling W. Validation study of alternatives to the Draize eye irritation test in Germany: Cytotoxicity testing and HET-CAM test with 136 industrial chemicals. Toxicol Vitro Int J Publ Assoc BIBRA. 1993 Jul;7(4):505–10.

33. Collado-González M, González Espinosa Y, Goycoolea FM. Interaction Between Chitosan and Mucin: Fundamentals and Applications. Biomimetics [Internet]. 2019 Apr 25.

34. Mazzarino L, Travelet C, Ortega-Murillo S, Otsuka I, Pig-not-Paintrand I, Lemos-Senna E, Borsali R. Elaboration of chitosan-coated nanoparticles loaded with curcumin for mu-coadhesive applications. J Colloid Interface Sci. 2012 Mar 15;370(1):58–66.

35. Belgamwar V, Shah V, Surana SJ. Formulation and evalua-tion of oral mucoadhesive multiparticulate system containing metoprolol tartarate: an in vitro-ex vivo characterization. Curr Drug Deliv. 2009 Jan;6(1):113–21.

36. Rojas S, Gispert JD, Abad S, Buaki-Sogo M, Victor VM, Gar-cia H, Herance JR. In vivo biodistribution of amino-functionalized ceria nanoparticles in rats using positron emis-sion tomography. Mol Pharm. 2012 Dec 3;9(12):3543–50.

37. Pérez-Campaña C, Gómez-Vallejo V, Martin A, Sebastián ES, Moya SE, Reese T, Ziolo R, Llop J. Tracing nanoparticles in vivo: a new general synthesis of positron emitting metal oxide nanoparticles by proton beam activation. Analyst. 2012 Oct 1;137(21):4902–6.

38. Fernández-Ferreiro A, Silva-Rodríguez J, Otero-Espinar FJ, González-Barcia M, Lamas MJ, Ruibal A, Luaces-Rodriguez A, Vieites-Prado A, Sobrino T, Herranz, M., García-Varela L, Blanco-Mendez J, Gil-Martínez M, Pardo M, Moscoso A, Medín-Aguerre S, Pardo-Montero J, Aguiar P. Positron Emission Tomography for the Development and Characterization of Corneal Permanence of Ophthalmic Pharmaceutical Formulations. Invest Ophthalmol Vis Sci. 2017 01;58(2):772–80.

39. The Association for Research in Vision and Ophthalmology Statement for the Use of Animals in Ophthalmic and Vision Research [Internet].

40. Burden N, Aschberger K, Chaudhry Q, Clift MJD, Doak SH, Fowler P, Johnston H, Landsiedel R, Rowland J, Sotne V. The 3Rs as a framework to support a 21st century approach for nanosafety assessment. Nano Today. 2017 Feb 1;12:10–3.

41. Loening AM, Gambhir SS. AMIDE: a free software tool for multimodality medical image analysis. Mol Imaging. 2003 Jul;2(3):131–7.

42. Zhang Y, Huo M, Zhou J, Xie S. PKSolver: An add-in program for pharmacokinetic and pharmacodynamic data analysis in Microsoft Excel. Comput Methods Programs Biomed. 2010 Sep;99(3):306–14.

43. Csaba N, Garcia-Fuentes M, Alonso MJ. The performance of nanocarriers for transmucosal drug delivery. Expert Opin Drug Deliv. 2006 Jul;3(4):463–78.

44. Oyarzun-Ampuero FA, Brea J, Loza MI, Torres D, Alonso MJ. Chitosan-hyaluronic acid nanoparticles loaded with heparin for the treatment of asthma. Int J Pharm. 2009 Nov 3;381(2):122–9.

45. Schiffelers RM, Woodle MC, Scaria P. Pharmaceutical prospects for RNA interference. Pharm Res. 2004 Jan;21(1):1–7.

46. Aktaş Y, Andrieux K, Alonso MJ, Calvo P, Gürsoy RN, Cou-vreur P, Capan Y. Preparation and in vitro evaluation of chitosan nanoparticles containing a caspase inhibitor. Int J Pharm. 2005 Jul 25;298(2):378–83.

47. Mahmoud AA, El-Feky GS, Kamel R, Awad GEA. Chitosan/sulfobutylether-β-cyclodextrin nanoparticles as a potential approach for ocular drug delivery. Int J Pharm. 2011 Jul 15;413(1–2):229–36.

48. Sohrabi SM, Niazi A, Chahardoli M, Hortamani A, Setoodeh P. In silico investigation of lactoferrin protein characterizations for the prediction of anti-microbial properties. Mol Biol Res Commun. 2014 Jun;3(2):85–100.

49. Tantra R, Tompkins J, Quincey P. Characterisation of the de-agglomeration effects of bovine serum albumin on nanoparticles in aqueous suspension. Colloids Surf B Biointerfaces. 2010 Jan 1;75(1):275–81.

50. Krauland AH, Alonso MJ. Chitosan/cyclodextrin nanoparticles as macromolecular drug delivery system. Int J Pharm. 2007 Aug 1;340(1–2):134–42.

51. Abdelkader H, Fathalla Z, Moharram H, Ali TFS, Pierscionek B. Cyclodextrin Enhances Corneal Tolerability and Reduces Ocular Toxicity Caused by Diclofenac. Oxid Med Cell Longev. 2018;2018:52609-76.

52. Partheniades E. Chapter 3 - Forces between Clay Particles and the Process of Flocculation. In: Partheniades E, editor. Cohesive Sediments in Open Channels [Internet]. Boston: Butter-worth-Heinemann; 2009 [cited 2020 Jun 24]. p. 47–88.

53. Sreekumar S, Goycoolea FM, Moerschbacher BM, Rivera-Rodriguez GR. Parameters influencing the size of chitosan-TPP nano- and microparticles. Sci Rep. 2018 Dec;8(1):46-95.

54. Saw CLL, Heng PWS, Liew CV. Chick Chorioallantoic Membrane as an In Situ Biological Membrane for Pharmaceutical Formulation Development: A Review. Drug Dev Ind Pharm. 2008 Jan 1;34(11):1168–77.

55. Kean T, Thanou M. Biodegradation, biodistribution and toxicity of chitosan. Adv Drug Deliv Rev. 2010 Jan 31;62(1):3–11.

56. Olmsted SS, Padgett JL, Yudin AI, Whaley KJ, Moench TR, Cone RA. Diffusion of macromolecules and virus-like particles in human cervical mucus. Biophys J. 2001 Oct;81(4):1930–7.

57. das Neves J, Bahia MF, Amiji MM, Sarmento B. Mucoad-hesive nanomedicines: characterization and modulation of mucoadhesion at the nanoscale. Expert Opin Drug Deliv. 2011 Aug;8(8):1085–104.

58. de Campos AM, Diebold Y, Carvalho ELS, Sánchez A, Alonso MJ. Chitosan nanoparticles as new ocular drug deliv-ery systems: in vitro stability, in vivo fate, and cellular toxici-ty. Pharm Res. 2004 May;21(5):803–10.

59. Sarmento B, das Neves J. Chitosan-Based Systems for Biopharmaceuticals: Delivery, Targeting and Polymer Therapeu-tics [Internet]. [cited 2020 Mar 24].

60. Takeuchi H, Thongborisute J, Matsui Y, Sugihara H, Yamamo-to H, Kawashima Y. Novel mucoadhesion tests for polymers and polymer-coated particles to design optimal mucoadhesive drug delivery systems. Adv Drug Deliv Rev. 2005 Nov 3;57(11):1583–94.

61. Jintapattanakit A, Junyaprasert VB, Kissel T. The role of mu-coadhesion of trimethyl chitosan and PEGylated trimethyl chitosan nanocomplexes in insulin uptake. J Pharm Sci. 2009 Dec 1;98(12):4818–30.

62. Allmeroth M, Moderegger D, Gündel D, Buchholz H-G, Mohr N, Koynov K, Rösch F, Thews O, Zentel R. PEGylation of HPMA-based block copolymers enhances tumor accumula-tion in vivo : A quantitative study using radiolabeling and positron emission tomography. J Controlled Release. 2013 Nov;172(1):77–85.

63. Varela-Fernández R, Díaz-Tomé V, Luaces-Rodríguez A, Con-de-Penedo A, García-Otero X, Luzardo-Álvarez A, Fernández-Ferreiro A, Otero-Espinar FJ. Drug Delivery to the Posterior Segment of the Eye: Biopharmaceutic and Pharmacokinetic Considerations. Pharmaceutics. 2020 Mar 16;12(3): 269.

64. Fàbregas A, Miñarro M, García-Montoya E, Pérez-Lozano P, Carrillo C, Sarrate R, Sánchez N, Ticó JR, Suñé-Negre JM. Impact of physical parameters on particle size and reaction yield when using the ionic gelation method to obtain cationic polymeric chitosan-tripolyphosphate nanoparticles. Int J Pharm. 2013 Mar 25;446(1–2):199–204.

65. Morris GA, Castile J, Smith A, Adams GG, Harding SE. The effect of prolonged storage at different temperatures on the particle size distribution of tripolyphosphate (TPP) – chitosan nanoparticles. Carbohydr Polym. 2011 Apr 2;84(4):1430–4.

GRAPHICAL ABSTRACT